NONLINEAR ANALYSIS OF REINFORCED CONCRETE FRAME STRUCTURES

A THESIS SUBMITTED TO
THE GRADUATE SCHOOL OF NATURAL SCIENCES
OF
MIDDLE EAST TECHNICAL UNIVERSITY

BY

GÜÇLÜ KORAY ÇİFTCİ

IN PARTIAL FULFILLMENT OF THE REQUIREMENTS
FOR
THE DEGREE OF MASTER OF SCIENCE
IN
CIVIL ENGINEERING

JANUARY 2013

Approval of the thesis:

NONLINEAR ANALYSIS OF REINFORCED CONCRETE FRAME STRUCTURES

Submitted by **GÜÇLÜ KORAY ÇİFTCİ** in partial fulfillment of the requirements for the degree of **Master of Science in Civil Engineering Department, Middle East Technical University** by,

Prof. Dr. Canan Özgen   _____
Dean, Graduate School of **Natural and Applied Sciences**

Prof. Dr. Ahmet Cevdet Yalçıner   _____
Head of Department, **Civil Engineering**

Assoc. Prof. Dr. Mustafa Uğur Polat   _____
Supervisor, **Civil Engineering Dept., METU**

Assoc. Prof. Dr. Özgür Kurç   _____
Co-Supervisor, **Civil Engineering Dept., METU**

Examining Committee Members:

Prof. Dr. Mehmet Utku   _____
Civil Engineering Dept., METU

Assoc. Prof. Dr. Mustafa Uğur Polat   _____
Civil Engineering Dept., METU

Assoc. Prof. Dr. Özgür Kurç   _____
Civil Engineering Dept., METU

Prof. Dr. Süha Oral   _____
Mechanical Engineering Dept., METU

Assoc. Prof. Dr. Alp Caner   _____
Civil Engineering Dept., METU

           Date: _____

I hereby declare that all information in this document has been obtained and presented in accordance with academic rules and ethical conduct. I also declare that, as required by these rules and conduct, I have fully cited and referenced all material and results that are not original to this work.

Name, Last name: Güçlü Koray Çiftci

Signature:

ABSTRACT

NONLINEAR ANALYSIS
OF
REINFORCED CONCRETE FRAME STRUCTURES

Çiftci, Güçlü Koray
M.Sc. in Department of Civil Engineering
Supervisor: Assoc. Prof. Dr. Mustafa Uğur Polat

January 2013; 57 Pages

Reinforced concrete frames display nonlinear behavior both due to its composite nature and the material properties of concrete itself. The yielding of the reinforcement, the non-uniform distribution of aggregates and the development of cracks under loading are the main reasons of nonlinearity. The stiffness of a frame element depends on the combination of the modulus of elasticity and the geometric properties of its section - area and the moment of inertia. In practice, the elastic modulus is assumed to be constant throughout the element and the sectional properties are assumed to remain constant under loading.

In this study, it is assumed that the material elasticity depends on the reinforcement ratio and its distribution over the section. Also, the cracks developing in the frame element reduces the sectional properties. In case of linear analysis, the material and sectional parameters are assumed to be constant. In practice, the modulus of elasticity E is a predefined value based on previous experiments and the moment of inertia I is assumed to be constant throughout the analysis. However, in this study, E and I are assumed to be combined. In other words, they cannot be separated from each other throughout the analysis. These two parameters are handled as a single parameter as EI. This parameter is controlled by the reinforcement ratio and its configuration, sectional properties and deformation of the member.

Two types of analysis, namely a sectional and a finite element analyses, are used in this study. From the sectional analysis, the parameter EI is calculated based on the sectional geometry, material properties and the axial load applied on the section. The parameter EI is then used in the finite element analysis to calculate the sectional forces and the nodal displacements. For the nonlinear analysis, the Newton-Raphson iterative approach is followed until convergence is obtained.

Keywords: Reinforced concrete frame, nonlinear analysis, sectional analysis, Finite Element Method, Newton Raphson Method.

ÖZ

BETONARME ÇERÇEVELİ
YAPILARIN LİNEER OLMAYAN ANALİZİ

Çiftci, Güçlü Koray
Yüksek Lisans, İnşaat Mühendisliği Bölümü
Tez Yöneticisi: Doç.Dr. Mustafa Uğur Polat

Ocak 2013; 57 Sayfa

Betonarme çerçeveler kompozit yapısından ve betonun malzeme özelliklerinden dolayı doğrusal olmayan bir davranış gösterirler. Agregaların düzensiz dağılımı ve yükleme altında çatlakların gelişimi doğrusal olmayan davranışın başlıca nedenleridir. Bir çerçevenin rijitliği, elastisite modülüne ve eleman kesitlerinin geometrik özelliklerine bağlıdır. Uygulamada, elastisite modülünün eleman boyunca sabit olduğu, kesit özelliklerinin de yükler altında değişmediği kabul edilir.

Elastisite modülü demir donatılarının eleman boyunca dağılımına ve kesit içindeki yerleşimine bağlıdır. Yükleme nedeniyle eleman üzerinde oluşan çatlaklar kesit özelliklerini azaltır. Bu çalışmada elastisite modülü (E) ve atalet momenti (I) parametreleri analiz boyunca tek bir parametre olarak düşünülmüştür. Doğrusal analiz için malzeme ve kesit parametreleri sabit olarak düşünülür. Genellikle E parametresi deneyler sonucunda hesaplanmış ortalama bir değer olup, I parametresi ise analiz boyunca sabit olarak kabul edilen teorik bir değerdir. Fakat bu çalışmada elastisite modülü ve atalet momenti tek bir parametre, yani EI olarak ele alınmıştır. Bu parametre donatının eleman içindeki yerleşimine, miktarına ve elemanın maruz kaldığı eksenel yüke göre değişir.

Hesaplamalarda kesit analizi ve sonlu elemanlar yöntemi kullanılmıştır. Kesit analizinde eksenel yük, donatı dağılımı ve kesitin geometrik özellikleri kullanılarak EI parametresi hesaplanmıştır.Hesaplanan bu parametreler kullanılarak sonlu elemanlar yöntemi ile eleman kuvvetleri ve sehim miktarları hesaplanmıştır. Doğrusal olmayan analizi, Newton Raphson yöntemi kullanılarak gerçekleştirilmiştir.

Anahtar Kelimeler: Betonarme çerçeve, lineer olmayan analiz, kesit analizi, Sonlu Elemanlar Yöntemi, Newton-Raphson yöntemi.

To my dearest wife and my family

ACKNOWLEDGEMENTS

TABLE OF CONTENTS

x

LIST OF TABLES

LIST OF FIGURES

LIST OF SYMBOLS

SYMBOLS

ε_c : Strain of concrete

ε_{co} : Peak strength strain of concrete

ε_{cu} : Failure strain of concrete

σ_c : Stress of concrete

f_c : Strength of concrete

M : Moment of a section

κ : Element curvature

r : Radius of concrete

NA : Neutral axis

s_t : Top steel

s_b : Bottom steel

b : Width of a section

h : Height of a section

ε_t : Strain of top fiber of the section

ε_b : Strain of bottom fiber of the section

f_{st} : Force applied by top steel

f_{sb} : Force applied by bottom steel

f_N : Force applied by axial force

$[N]$: Shape functions

$[B]$: Strain-displacement matrix

$[K]$: Stiffness matrix

$\bar{u}$: Displacements of the nodes

u : Axial displacement of the nodes

v : Transverse displacements of the nodes

θ : Rotational displacements of the nodes

w : Weight of integration points

A : Area of the section

E_s : Elastic modulus of steel

f_y : Yield strength of steel

ϕ : Diameter of reinforcing steel

E : Modulus of elasticity of frame

I : Moment of inertia of the section

CHAPTER 1

INTRODUCTION

1.1   General

A linear analysis is suitable when a structure is expected to behave in a linearly manner, i.e., obeys Hooke's Law. Linearly proportioned stress-strain relationship and returning to its original shape once the load is removed are the assumptions. Linear analysis is accepted sufficient in design of standard buildings. Also, it has advantages in terms of number of parameters used, idealized material behavior and straight forward solution within a reasonable time.

On the other hand, a nonlinear analysis is essential when a structure is expected to be loaded beyond the elastic limits of the materials. In this type of analysis, the material experiences plastic deformation and there is no possibility of returning to its original shape. It requires more detailed material models and more time for analysis, due to its iterative approach.

Nonlinear structural behavior arises from 3 causes: boundary condition nonlinearity, geometric nonlinearity and material nonlinearity.

Reinforced concrete is a very complex composite material resulting from a combination of two materials, concrete and steel, both of which have entirely different mechanical properties. Although the literature on concrete and reinforced concrete is mainly based on elastic parameters such as proportional limit and modulus of elasticity, the behavior of reinforced concrete cannot be modeled properly by linear elastic behavior assumptions. Actually, the resulting composite material behaves in an elasto-plastic manner responding differently to tensile and compressive stresses. Concrete has a small capacity in tension, but usually, for the sake of simplicity, the tension capacity of the concrete is neglected.

In a frame structure flexural members are subjected to transverse loads, causing bending moment and shear force. For instance, in a fixed end beam element, tension develops both in the fix end zone and in the span, at the top and at the bottom of the section, respectively. In the design step of a concrete beam, the tension zones are provided by reinforcing bars to resist the tensile forces. For example standard beam design is shown in Figure 1.1. The EI parameter is calculated at each section (s1, s2, s3 …) and combined to obtain overall EI of the beam.
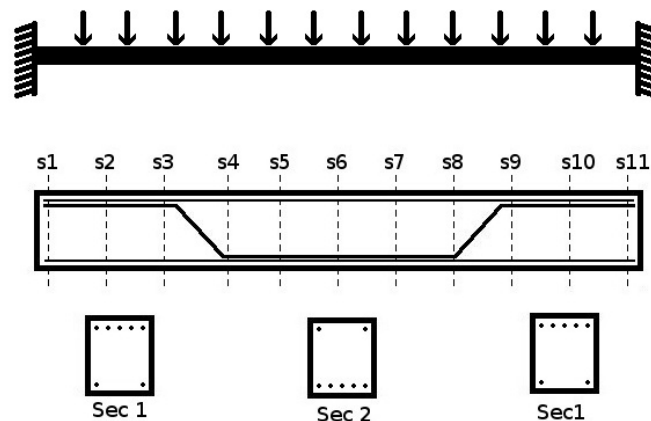
Figure 1.1 Change of reinforcement layout throughout the beam

At each section, the curvature of the frame is approximated by shape functions, i.e., the Hermitian shape functions. Then, the rate of change of sectional moments with respect to section curvature under axial load is calculated, in other words, the EI parameter. Numerical integration of the EI parameters throughout the section equals to the reinforced concrete elements' EI.

In linear analysis, it is assumed that the displacements fall within the linear range. Thus, no yielding is expected at steel members. Also, the concrete can encounter some minor cracking, but not crushing of the concrete. On the other hand, in nonlinear analysis reinforcing bars can yield or some portion of the concrete may be crushed. The section may undergo fiber to fiber redistribution. Under bending moments, the top fiber of the beam reaches the peak stress level for concrete. The top fiber cannot carry more loading, thus it reduces its stress and peak stress is carried by lower fibers. This allows to compression section carry more load.

1.2   Purpose

The goal of this thesis is to focus on nonlinear analysis of reinforced concrete frame by a computer program that updates stiffness of the elements according to their deformations. In this study, material nonlinearity is assumed to be the main reason of the nonlinear behavior. The program uses finite element method to analyze the given reinforced concrete frame. Finite element method is a commonly used method for structural analysis. Two node beam element is selected as a finite element model and the moment curvature analysis is used to obtain the sectional behavior of the reinforced concrete beam. The two node beam element is formulated for linear behavior, thus nonlinear solution is implemented by iterative approach and using a high density mesh.

Under various loadings the element yields and the yielding of an element results in the formation of plastic hinges. The formation of plastic hinges causes redistribution of forces among the members. The goal of this study is to model the yielding and the redistribution behavior of the elements.

1.3   Previous Studies

Reinforced concrete is one of the most preferred materials in construction industry, so understanding of the behavior is rather important. There are a lot of material models available in the literature for both concrete and steel. However, in order to get the accurate perception, selection of appropriate model is crucial.

To start with, steel can be modeled either hardening or no hardening material. Bilinear models are accurate enough to model steel behavior (Figure 1.2).
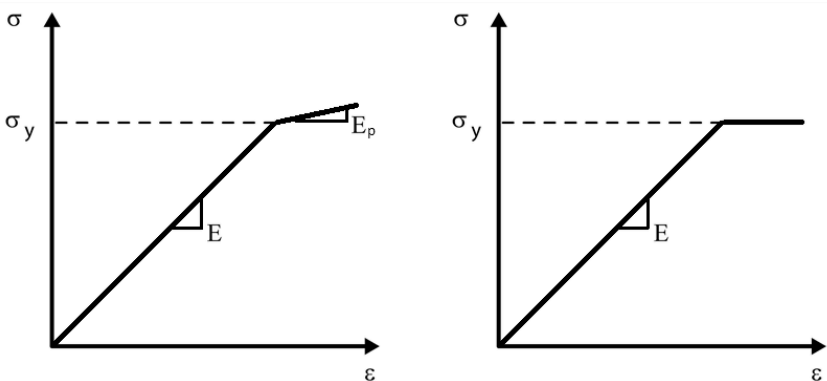
Figure 1.2 Steel models with and without hardening

On the other hand, behavior of concrete is complex when compared to steel's behavior. Unlike steel, concrete has a very low capacity of carrying tension. Most of the time, it is assumed that it cannot carry tension at all. The behavior under compression is modeled by

combination of curves with different orders. Early assumptions are shown in figure 1.3 for flexural analysis and in 1951 E. Hognestad [1] generates a formula (1.1) that covers the behavior of concrete (Figure 1.4).
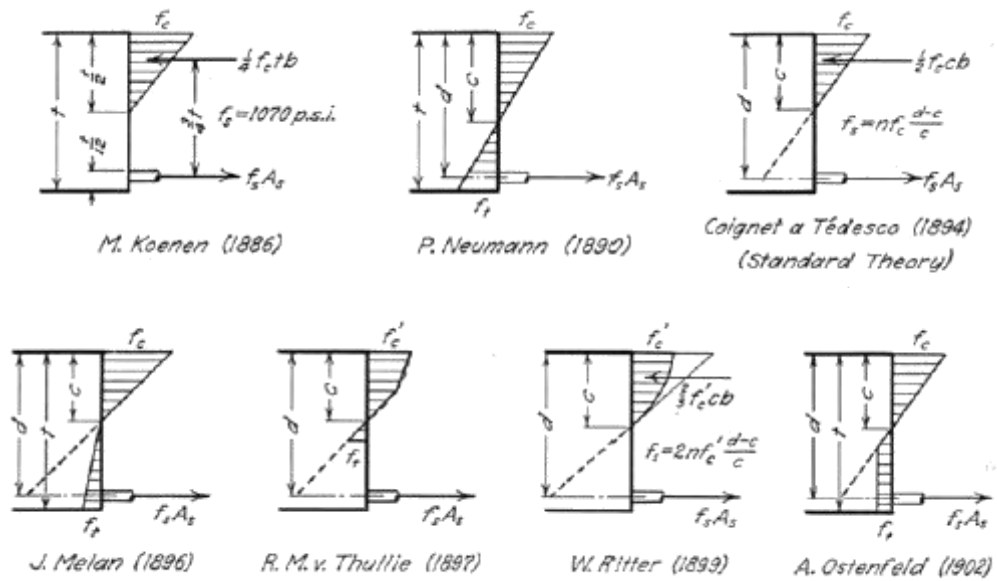
Figure 1.3 Early assumptions for flexural analysis

$$\sigma c = fc\left[\frac{2\varepsilon_c}{\varepsilon_{co}} - \left(\frac{2\varepsilon_c}{\varepsilon_{co}}\right)^2\right] if\ 0 \le \varepsilon_c < \varepsilon_{co}$$

$$\sigma c = fc\left[1 - 0.15\left(\frac{\varepsilon_c - \varepsilon_{co}}{\varepsilon_{cu} - \varepsilon_{co}}\right)\right] if\ \varepsilon_{co} \le \varepsilon_c < \varepsilon_{cu}$$

(1.1)
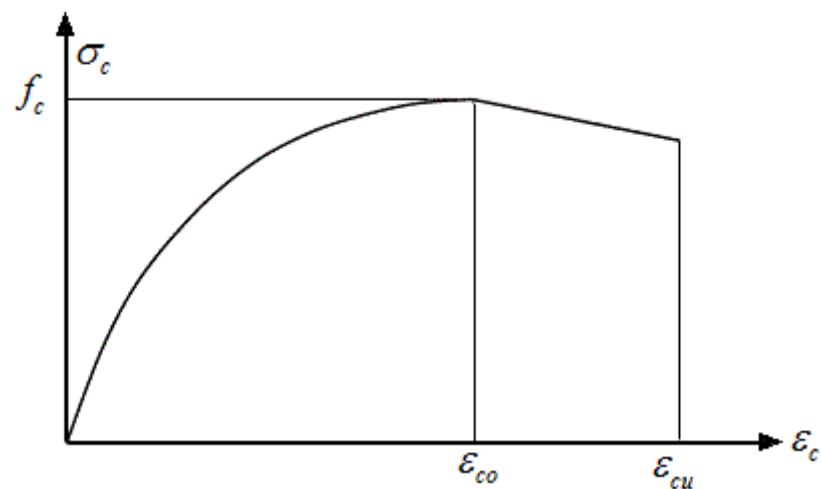
Figure 1.4 Hognestad Parabola

3

Ngo and Scordelis [2] are the pioneers in the usage of finite element method on reinforced concrete structures. They analyzed simple beams by using constant strain triangular elements. Both concrete and reinforcements are modeled by constant strain triangular elements. The concrete and the steel elements are connected to each other with zero length bond elements at discrete points. The material models used in this study are assumed to be linear. The cracks on the concrete are modeled by separating the elements connections on the crack line. Two overlapping nodes are assigned on the cracked elements, allows moving individually. They have concluded that the bond stresses at cracked node is zero.

Cracking of concrete is one of the most important reasons of nonlinearity. Nilson [3] uses an incremental load method to analyze nonlinearity of concrete and reinforcement. Instead of Ngo and Scordelis, Nilson uses nonlinear element models. Four constant strain triangle elements are combined to form a quadrilateral element and the central node is condensed out. To implement cracking behavior, when a quadrilateral element is cracked the solution is broken and forces on that element is omitted and then iterations continue.

In 1983, Gupta A.K. and Akbar H. [4] studied this subject by using quadrilateral isoparametric element and developed a formulation suitable for modeling cracks in reinforced concrete structures. Cracking of concrete is the main source of the material nonlinearity. They proposed one point Gaussian quadrature for concrete instead of two, and θ the principal strain directions are defined by one point instead of four. Also, in that study, the crack direction was redefined as perpendicular to the principal direction, which changes as the stiffness of the concrete changes. They showed that the proposed formulation gives superior results as compared to both the standard isoparametric element and the conventional selectively integrated element.
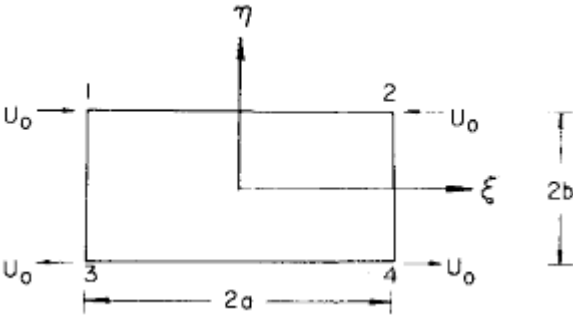
Figure 1.5 Rectangular Isoparametric Element

In 1990, H. G. Kwak and F. C. Filippou [5] dealt with the finite element analysis of RC structures under monotonic and cyclic loads. The concrete and the reinforcing bars modeled separately and combined with a bond-slip element. The smeared crack model is selected for the behavior of concrete. Also, the cracks on the concrete are modeled with rotating crack model, allowing to changing of crack direction with load history.
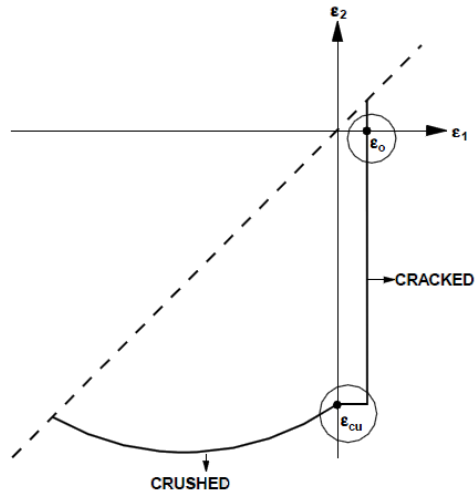
Figure 1.6 Strength Failure Envelope of Concrete

The bond-link element is selected because of its simplicity. To apply this model; firstly, the reinforcing bars should be located along the edge of a concrete element and secondly, a double node is required to measure the relative slip between concrete and reinforcing bars.
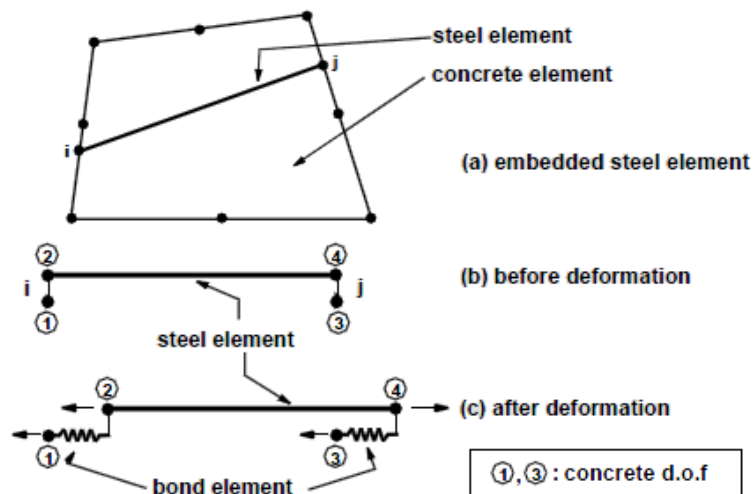
Figure 1.7 Reinforcing steel element with bond-slip

H. G. Kwak and Filip C. Filippou has concluded that, the proposed reinforced concrete model gives successive results with the experiments and the tension stiffening plays an important role in the analysis of RC beams under monotonic loads.

In 2000, H. G. Kwak and Sun-Pil Kim [6] studied on the nonlinear analysis of RC beams, based on moment curvature relation. Their aim is to describe the behavior of the reinforced concrete structures under overload conditions and to estimate RC beams' ultimate strength accurately. Their study tries to describe the bond slip behavior of the reinforcements. Bond slip effect can be described as the loosing contact of reinforcing bars with the concrete at the cracking path. The concrete cannot bear tension and cracks, whereas, the reinforcement keeps to elongate. The bond-link element requires a double node; however beam element has single degree of freedom at each end, so makes it impossible to use. To overcome this problem, the bond slip behavior is introduced by a numerical algorithm. After several analyses, they conclude that for over reinforced beams, the bond slip effect is negligible. On the other hand, the under reinforced beams, tension softening and bond slip effect have dominant effects on cracked zone.

In 2003, K. Phuvoravan [7] introduced a new finite element for the nonlinear analysis of RC slabs in his doctor of philosophy thesis. For concrete model a four-node Kirchhoff shell element is selected. The steel reinforcement bars are modeled by two-node Euler beam elements. In this new element, the location of the reinforcement bars were taken into account, so considered the effect of each individual bar. His approach allowed the modeling of progressive concrete cracking and he assumed perfect bond between concrete and steel during all loading stages. He included material nonlinearities in his model. Although his new finite element was applied to the finite element analysis of RC buildings, scope of his research was limited to flat slabs.

CHAPTER 2

ANALYSIS METHODS

2.1 Sectional Analysis

The deformed shape of a beam under bending moment M is shown in Figure 2.1. The curve AmB is called the deflection curve and κ is the curvature and r is the radius of curvature.
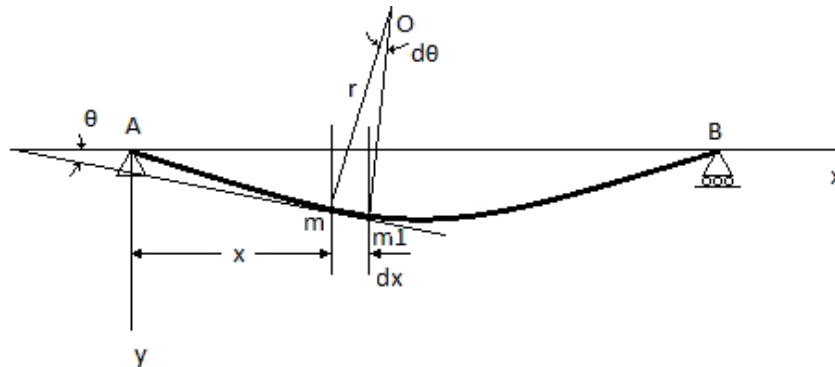
Figure2.1 Deflection curve of the beam

Relation between the curvature and the bending moment is

$$\frac{1}{r} = \kappa = \frac{M}{EI}$$

(2.1)

Rearranging the terms we obtain;

$$EI = \frac{M}{\kappa}$$

(2.2)

Equation 2.2 shows that if the moment capacity of a section is known for a given curvature, then EI of a section can be calculated.
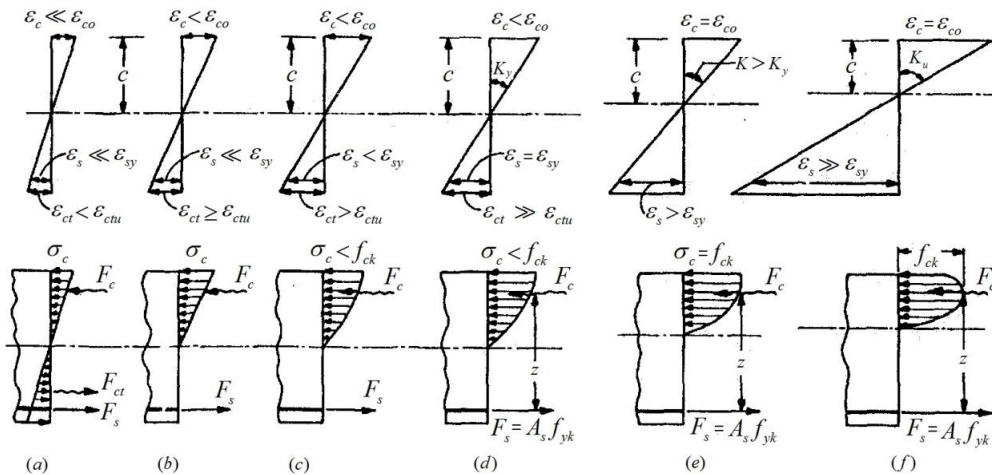
Figure 2.2 Change of depth of neutral axis

The stress distribution of a beam under bending moments is explained in U. Ersoy, G. Ozcebe and T. Tankut, "Reinforced Concrete", Ankara, 2003(pp. 197-198)[8].In Figure 2.2.a, the loading is very small and concrete in tension zone is still not cracked. Also, the behavior is in the linear range. In Figure 2.2.b, the bottom fiber reached its tensile capacity and cracked. After this limit, the concrete cannot carry tension. On the other hand, at the compression zone the behavior is still linear. If more flexural forces applied, the stress distribution becomes nonlinear (Figure 2.2.c). At further loading the reinforcing steel yields (Figure 2.2.d). Until this point, the neutral axis depth (c) stay stable. If the loading continues, the top fiber of the concrete reaches to its peak value f_{ck} (Figure 2.2.e). The reinforcing steel shows large deformations but, due to the strain distribution of the concrete section, the steel strains cannot be compensated. This cause to rise of neutral axis, in other words, c decreases to a certain amount. If the loading increases furthermore, the top fiber carries less stress but reaches its ultimate strain ε_{cu} (Figure 2.2.f). The section has reached its capacity and cannot carry more loading.

To calculate moment capacity of a RC section, the first step is to calculate neutral axis depth. It is assumed that the cross-section of the beam remain plane during bending. The sectional forces, which are concrete forces, steel forces and the axial force; should be in equilibrium, in other words, summation of them should be zero. In order to calculate concrete forces Hognestad concrete model is used. Usually concrete section is divided into several layers and for each layer the strains are calculated. The concrete model transforms the stresses to the strains. For each layer the stresses are multiplied by the area of each layer to obtain forces. This method has two drawbacks; firstly, the solution gives approximate results and secondly, the number of layers should be enough to obtain right behavior. In this study the section analysis is performed by using several integration points. The concrete model is Hognestad concrete model. The ascending part is a 2nd order polynomial and the descending part is a straight line. This means for the ascending part 3 points are enough to calculate if Simpsons' rule is used. And for the descending part two points are enough for exact integration. This method consumes less time compared to layering the section; however, the geometry of the section must be rectangular. Another drawback of this method is that it is optimized for Hognestad concrete model. Since in this study only rectangular sections are considered and the concrete model is selected as Hognestad concrete model, these drawbacks do not affect the analysis.

Two natural axis depth guesses, c1 and c2 are made. The first guess assumes the neutral axis depth is at top face, where c1 equals to 0. And the second guess assumes the neutral axis depth at the bottom face, where c2 equals to h. Since the total force versus neutral axis depth is a continuous function, the exact neutral axis depth can be calculating by bisection method. By interpolating between these two guesses, a new estimate is calculated. After several iterations the neutral axis depth is approximated.

After the calculation of the neutral axis depth, the section moment is calculated with respect to mid depth of section. It is assumed that the axial force applied to the section acted in the geometrical center of the section (Figure2.3).
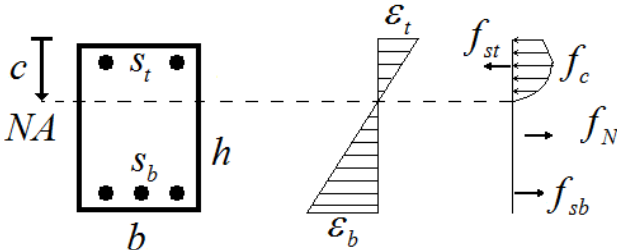
Figure 2.3 Calculation of sectional forces

Curvatures are calculated by nodal displacements and they will be examined in sec 2.2. The rate of change of moment capacity of a section with respect to curvature equals to EI as

described in equation 2.2. In other words, it is the slope of moment curvature diagram at a given curvature.
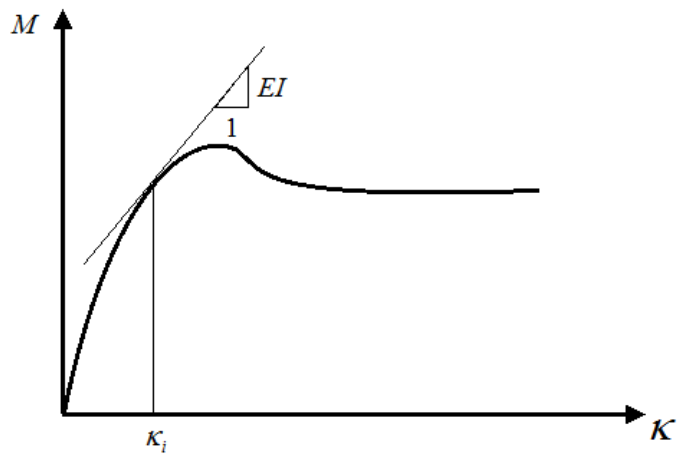
Figure 2.4 Moment curvature diagram of an arbitrary section

In the structural analysis, the EI of the member should always be positive. However, the slope of the moment curvature sometimes may be negative. To overcome this problem, the slope of the moment curvature diagram is assumed to be a small non-negative value. If the EI gets zero or negative values, the solution does not converge.

2.2 Finite Element Method

Two-node beam element is selected as the finite element model in this study, having four degrees of freedom; one lateral and one rotational at each node. Two-node bar element is added to this model to have six degree of freedom system (Figure2.5).
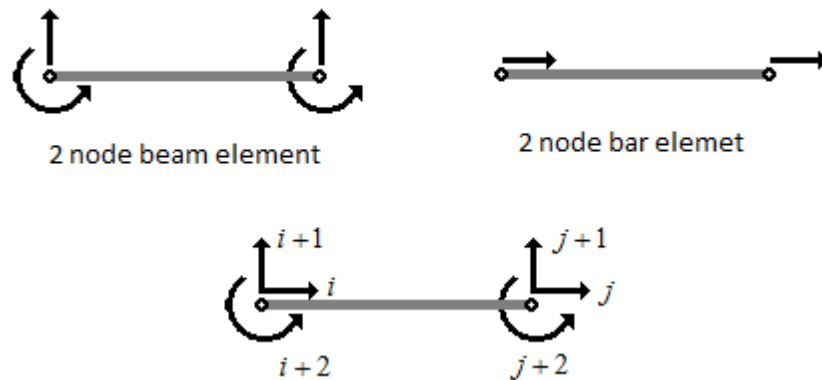
Figure 2.5 Degrees of freedom of the beam element

Hermitian shape functions are used for the two-node beam element (Equation2.3).
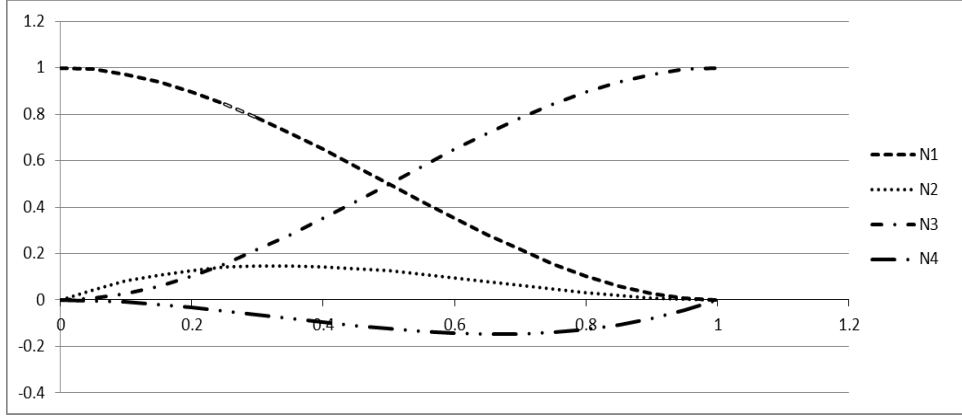
Figure 2.6 Hermitian Function

$$N_1 = 1 - 3\left(\frac{x}{L}\right)^2 + 2\left(\frac{x}{L}\right)^3 \qquad N_2 = x\left(1 - \frac{x}{L}\right)^2$$

$$N_3 = 3\left(\frac{x}{L}\right)^2 - 2\left(\frac{x}{L}\right)^3 \qquad N_4 = x\left[\left(\frac{x}{L}\right)^2 - \frac{x}{L}\right] \qquad (2.3)$$

The second derivative of the shape functions is called the strain-displacement matrix and calculated as shown in equation 2.4:

$$[B] = \frac{d^2}{dx^2}[N]$$

$$B_1 = -6\frac{(L-2x)}{L^3} \qquad B_2 = -2\frac{(2L-3x)}{L^2}$$

$$B_3 = 6\frac{(L-2x)}{L^3} \qquad B_4 = -2\frac{(L-3x)}{L^2} \qquad (2.4)$$

For the straight beam the stiffness is calculated as:

$$[k] = \int_0^L [B]^T EI [B] dx \qquad (2.5)$$

The element stiffness matrix $[k]$ is 4 by 4 matrix and EI parameter is obtained from the slope of the moment curvature diagram. Integration over the length of the element is converted to a numerical integration. Gaussian Quadrature is selected as the integration method. At each integration point, the EI parameter is calculated and element stiffness's are summed up by multiplying their weights.

Curvature (κ) is the second derivative of the displacements ($\overline{u}$), as seen in Equation 2.6.

$$\kappa = \frac{d^2\overline{u}}{dx^2} \qquad (2.6)$$

$$u(x) = [\overline{u}]_{1\times4}[N]_{4\times1} = \overline{u}_{11}N_{11} + \overline{u}_{12}N_{21} + \overline{u}_{13}N_{31} + \overline{u}_{14}N_{41} \qquad (2.7)$$

$$\kappa(x) = [\overline{u}]_{1\times4}[B]_{4\times1} = \overline{u}_{11}B_{11} + \overline{u}_{12}B_{21} + \overline{u}_{13}B_{31} + \overline{u}_{14}B_{41} \qquad (2.8)$$

At each integration point (x_i) the curvatures (κ_i) and the corresponding EI_i are calculated. The stiffness matrix at corresponding integration point is:

$$[k_i] = [B]^T EI_i [B]$$

(2.9)

And the overall element stiffness is:

$$[k] = \sum_{i=1}^{n} [k_i] w_i = \begin{bmatrix} k_{11} & k_{12} & k_{13} & k_{14} \\ k_{21} & k_{22} & k_{23} & k_{24} \\ k_{31} & k_{32} & k_{33} & k_{34} \\ k_{41} & k_{42} & k_{43} & k_{44} \end{bmatrix}$$

(2.10)

In equation 2.10, w_i represents the weight of the integration point.

At this step a 4x4 stiffness matrix is constructed. The axial degrees of freedom are added to the system. The axial stiffness is calculated from the EI parameter assuming the moment of inertia of a rectangular section does not change. As the flexural stiffness softens via the displacements, also the axial stiffness decreases.

$$I = \frac{1}{12} bh^3$$

(2.11)

$$A = I \frac{12}{h^2}$$

(2.12)

$$EA = EI \frac{12}{h^2}$$

(2.13)

$$k_{bar} = \frac{EA}{L}$$

(2.14)

$$[K] = \begin{bmatrix} k_{bar} & 0 & 0 & -k_{bar} & 0 & 0 \\ 0 & k_{11} & k_{12} & 0 & k_{13} & k_{14} \\ 0 & k_{21} & k_{22} & 0 & k_{23} & k_{24} \\ -k_{bar} & 0 & 0 & k_{bar} & 0 & 0 \\ 0 & k_{31} & k_{32} & 0 & k_{33} & k_{34} \\ 0 & k_{41} & k_{42} & 0 & k_{43} & k_{44} \end{bmatrix}$$

(2.15)

2.3 Nonlinear Solution

In order to approach the real behavior of the reinforced concrete, rather than the approximate solutions with linear analysis, nonlinear analysis is preferred. Nonlinearity is achieved by updating element stiffness matrices with respect to nodal displacements. Newton Raphson Method is used for nonlinear analysis. The force is applied in several increments and these increments are equally divided. At each increment the iterations are performed until the convergence is achieved. If the iterations cannot converge, the applied load is divided into two. The reasons for non-convergence are either the element fails or the iterations are not enough. Decreasing load increments solves both of these problems. By this approach the failure load is determined.

In Figure 2.7, the Newton Raphson method is summarized. When the applied load is solved with initial tangent stiffness (K_0), the applied force and the internal force are not equal to each other. The difference is called unbalanced load and at each iteration the unbalanced load decreases. When the unbalanced loads are smaller than a tolerance, the solution is converged.
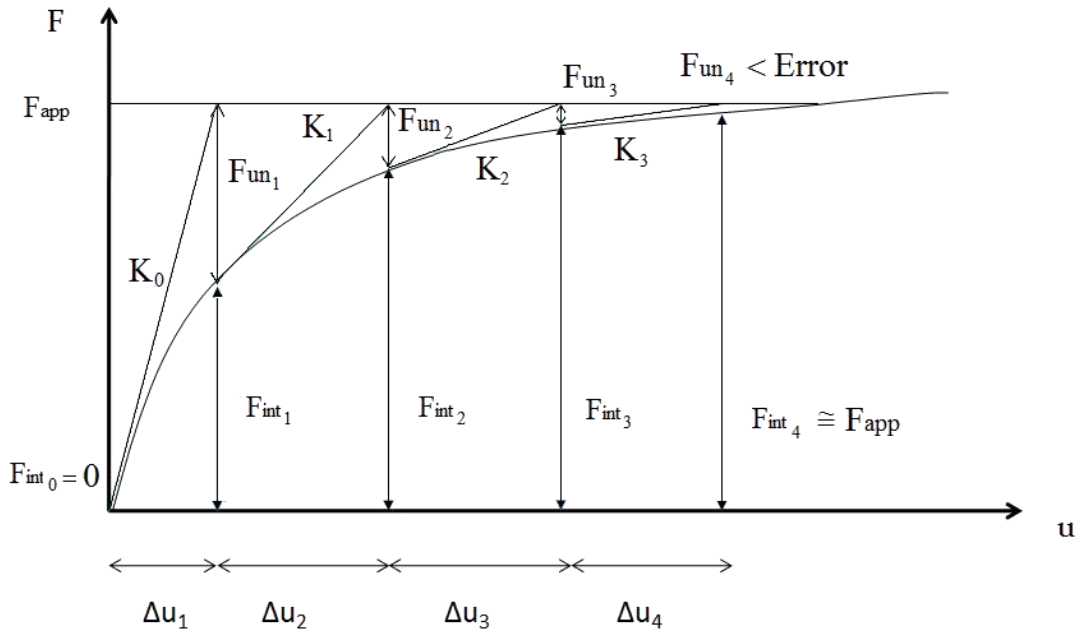
Figure 2.7 Newton Raphson Method for single increment

The Newton Raphson method calculates stiffness of the system for every iteration. To speed up this algorithm, Modified Newton Raphson method is generated. Instead of calculating stiffness at each iteration, the initial stiffness is used for the calculations. This causes to perform more iteration to reach convergence, but total time usually decreases.
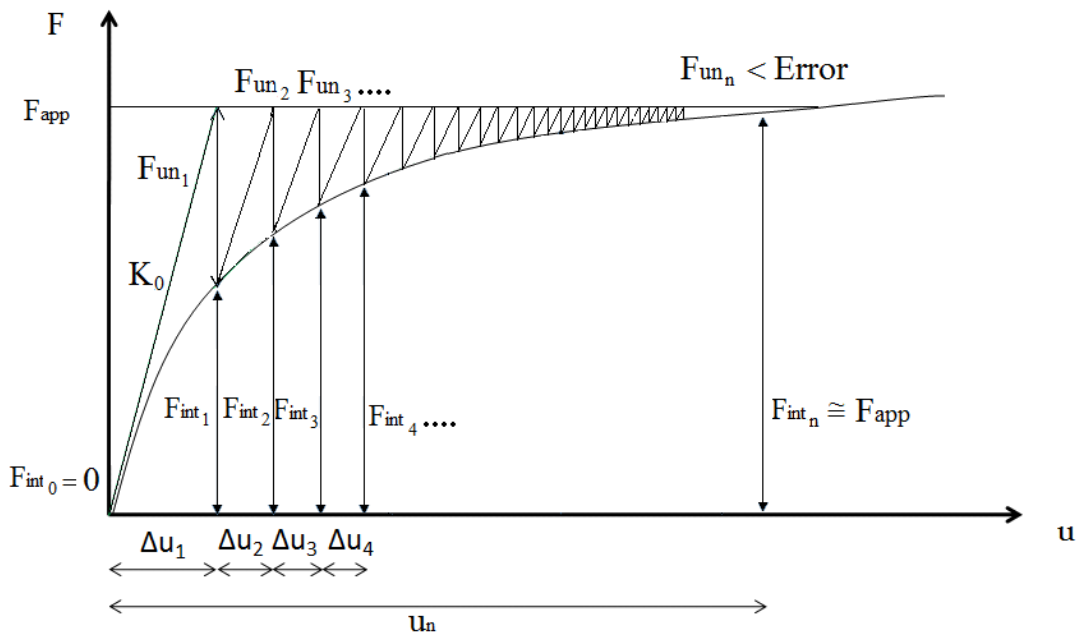
Figure 2.8 Modified Newton Raphson Method for single increment

As it can be seen in Figure 2.8, if the slope of the curve decreases very much, the iteration number increases significantly. The applied load can be divided into increments to further decrease computational time. At each increment the stiffness of the system calculated once. This will decrease the number of iterations.
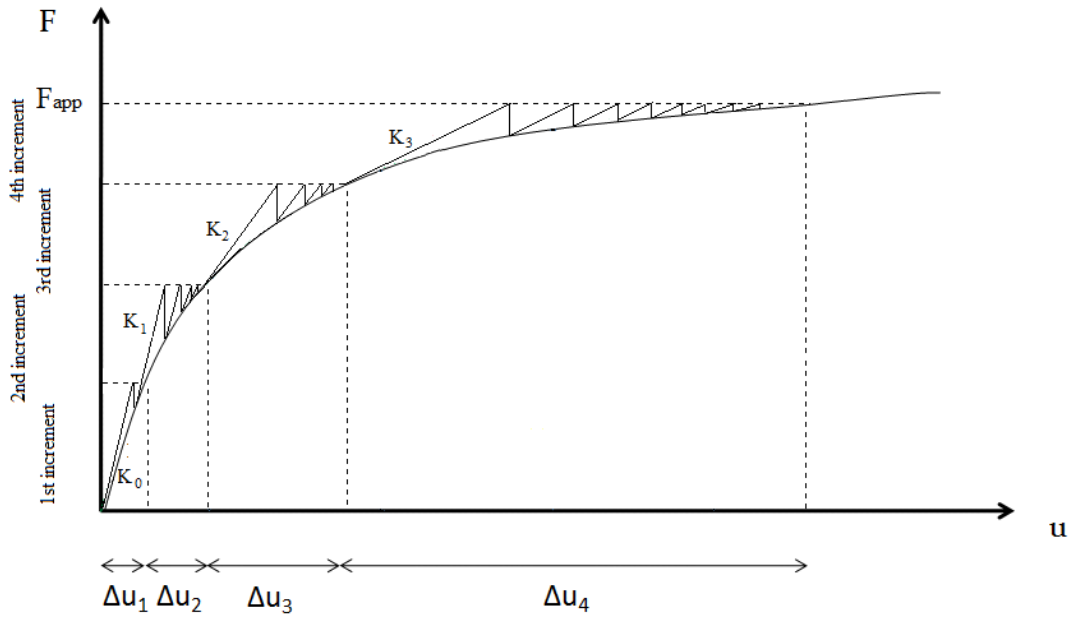
Figure 2.9 Modified Newton Raphson Method for multiple increments

CHAPTER 3

COMPUTER PROGRAM

3.1 Material Models

To define a reinforced concrete frame, firstly concrete and steel materials should be defined. Concrete is a non-homogenous material due to its ingredients, which is a mixture of cement, aggregate and water. The plain concrete has a negligible tensile strength and low ductility. Steel is a homogenous material and displays similar behavior under tension and compression. Reinforced concrete is a material which combines the positive characteristics of both concrete and steel, forming strong, ductile and durable material. In practice, linear analysis is preferred for reinforced concrete structures, assuming both the strains and displacements are small. However, in linear analysis case, neither the material nor the geometrical nonlinearities are considered.

3.1.1 Concrete Model

In this study, Hognestad concrete model is utilized. This model consists of two sections, the parabolic part and the linear part. ε_{co} is the strain level where the concrete reaches to its peak strength. ε_{cu} is the ultimate strain level of concrete where failure begins. Hognestad defines stress strain relationship of concrete by a second order parabola in 0 - ε_{co} range and by a linear descending part between ε_{co} and ε_{cu} (Figure3.1).
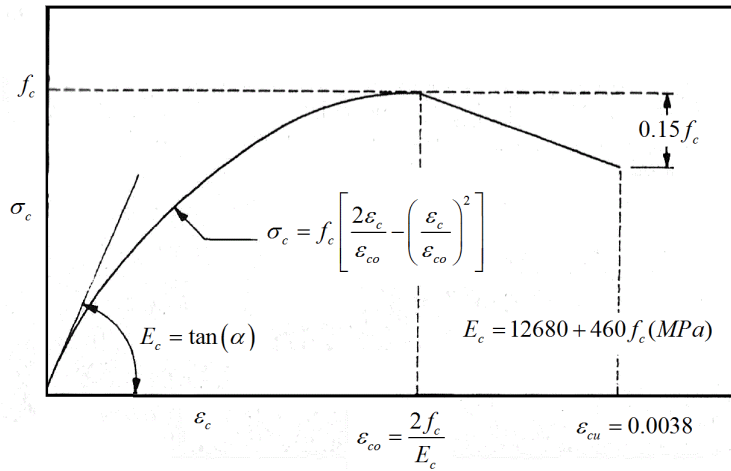
Figure 3.1 Hognestad Parabola

The equation of these parabola and line is given in equation 3.1a and3.1b

$$\sigma c = fc\left[\frac{2\varepsilon_c}{\varepsilon_{co}} - \left(\frac{2\varepsilon_c}{\varepsilon_{co}}\right)^2\right] if\ 0 \le \varepsilon_c < \varepsilon_{co}\tag{3.1a}$$

$$\sigma c = fc\left[1 - 0.15\left(\frac{\varepsilon_c - \varepsilon_{co}}{\varepsilon_{cu} - \varepsilon_{co}}\right)\right] if\ \varepsilon_{co} \le \varepsilon_c < \varepsilon_{cu}\tag{3.1b}$$

ε_{co} is assumed as a function of f_c and ε_{cu} is assumed to be 0.0038.

3.1.2 Steel Model

Steel is modeled in three different behaviors. The first one is modeled as a linearly elastic and perfectly plastic material in this study. Behavior of steel is modeled as a bilinear steel model without hardening (Figure3.2).
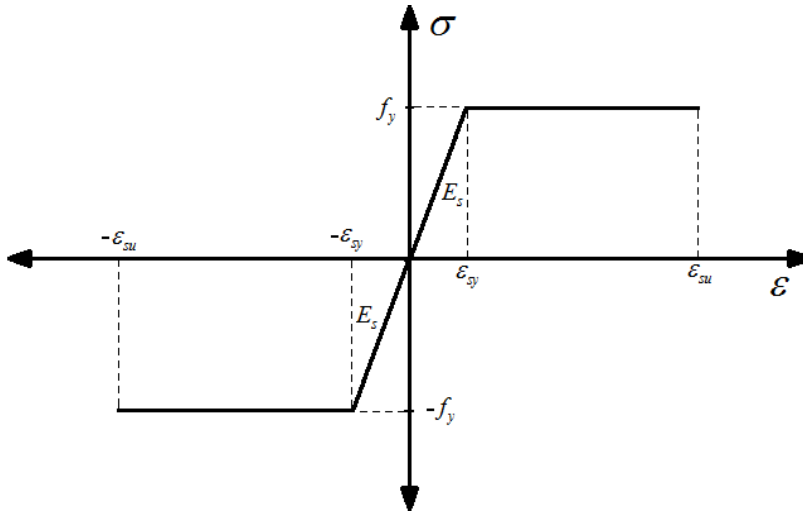
Figure 3.2 Bi-linear Steel Model

$$\sigma = E_s \varepsilon \qquad if \: |\varepsilon| < \varepsilon_{sy}$$

$$\sigma = f_y \frac{\varepsilon}{|\varepsilon|} \qquad if \: |\varepsilon| \le \varepsilon_{su} \: and \: |\varepsilon| \ge \varepsilon_{sy} \qquad \qquad (3.2)$$

$$\sigma = 0 \qquad if \: |\varepsilon| > \varepsilon_{su}$$

Second steel model is the tri-linear steel model with hardening (Figure 3.3). After a limited yielding plateau, the steel hardens until failure. There are three stages in this model. The elastic stage is between 0 and ε_{sy}. At ε_{sy}, the steel starts to yield until strain reaches to ε_{sh}. This region is called the yielding zone. The last stage is the hardening stage. It continues until failure.
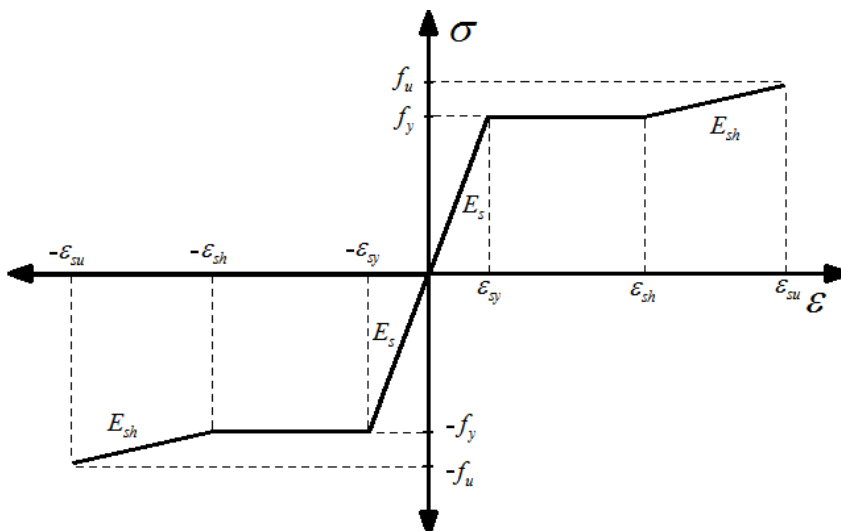
Figure 3.3 Steel Model for Tri-Linear Steel Model

$$\sigma = E_s \varepsilon \qquad if \ |\varepsilon| < \varepsilon_{sy} \qquad \sigma = f_y \frac{\varepsilon}{|\varepsilon|} \qquad if \ |\varepsilon| \leq \varepsilon_{sh} \ and \ |\varepsilon| \geq \varepsilon_{sy}$$

$$\sigma = f_y + \left(\left(f_u - f_y \right) / \left(\varepsilon_{su} - \varepsilon_{sh} \right) \right) \left(\varepsilon - \varepsilon_{sh} \right) \frac{\varepsilon}{|\varepsilon|} \qquad if \ |\varepsilon| \leq \varepsilon_{su} \wedge |\varepsilon| > \varepsilon_{sh}$$

$$\sigma = 0 \qquad if \ |\varepsilon| > \varepsilon_{su} \qquad\qquad\qquad (3.3)$$

The last steel model available in this program is the reinforcing steel model in Stress-Strain Model for Grade 275 Reinforcing Steel paper by K. J. Thompson and R. Park[9]. It has the same stages as the tri-linear steel model but instead of a straight line, a parabola is implemented for the hardening part.
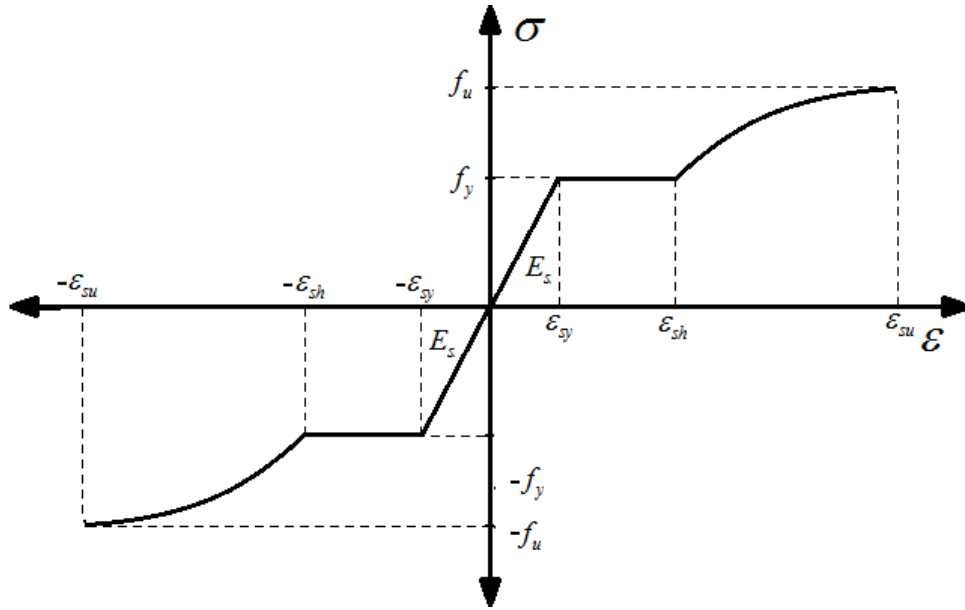
Figure 3.4 Steel Model for Reinforcing Steel

$$\sigma = E_s \varepsilon \qquad if \ |\varepsilon| < \varepsilon_{sy}$$

$$\sigma = f_y \frac{\varepsilon}{|\varepsilon|} \qquad if \ |\varepsilon| \leq \varepsilon_{sh} \wedge |\varepsilon| \geq \varepsilon_{sy}$$

$$\sigma = f_y \left(\frac{m \left(\varepsilon - \varepsilon_{sh} \right) + 2}{60 \left(\varepsilon - \varepsilon_{sh} \right) + 2} + \frac{\left(\varepsilon - \varepsilon_{sh} \right) \left(60 - m \right)}{2 \left(30q + 1 \right)^2} \right) \qquad if \ |\varepsilon| \leq \varepsilon_{su} \ and \ |\varepsilon| > \varepsilon_{sh}$$

$$where \qquad m = \frac{\left(f_u / f_y \right) \left(30q + 1 \right)^2 - 60q - 1}{15q^2}$$

$$and \qquad q = \varepsilon_u - \varepsilon_{sh} \qquad\qquad\qquad (3.4)$$

$$\sigma = 0 \qquad if \ |\varepsilon| > \varepsilon_{su}$$

3.2 Structure of the Program

To simulate a reinforced concrete frame behavior the model of the frame should be flexible and easy to use. The structures used in the program are:

- Joint
- Concrete Material
- Steel Material
- Reinforcement
- RC Section
- RC Member
- RC Frame

Joint

Joint defines the x-y coordinates of the degrees of freedom and the restraint information whether they are free to move or not.

Concrete Material

Concrete material stands for the strength of concrete (f_c), peak strain (ε_{co}) and ultimate strain (ε_{cu}). These parameters define the Hognestad parabola and used in the calculation of strength of a concrete at a given strain.

Steel Material

It holds the elasticity (E_s) and the yield strength (f_s) of the steel. With these two parameters a bilinear steel model is constructed and according to a given strain a stress value is calculated.

Reinforcement

It defines the properties of the reinforcement in concrete. It holds the steel type (f_s), diameter of a single bar (ϕ), depth of the steel bars (d) and the number of the bars (n) as seen in Figure 3.5.
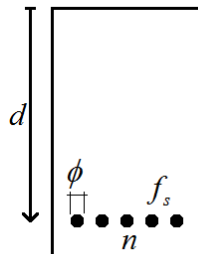
Figure 3.5 Definition of reinforcement structure

RC Section

The cross section of the element is defined in Figure 3.6. It holds the geometry of the section (b, h), the reinforcing bar groups inside the section (Rb1, Rb2, Rb3), properties of concrete material. Every reinforcing bar group may have different steel strengths.
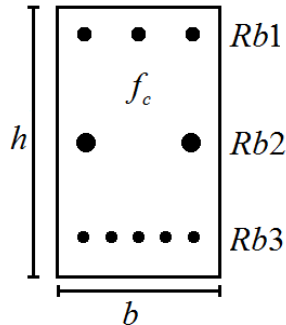
Figure 3.6 Definition of reinforced concrete section structure

RC Member

The reinforced concrete member is defined as a summation of several cross sections. Also a member should have start and end joints to assemble the system stiffness. For the finite element analysis it has six degrees of freedom, first three at start joint and last three at end joint. Cross section information is registered in this class of the program, in other words it defines which parts of the element has what kind of a section. The orientation and the length of the member are calculated from the start and end joints. The anchorage length should be taken into account during the modeling phase. In Figure 3.7 the properties of the RC member structure is defined. The dotted lines represent the anchorage length and these sections are not considered as reinforcement.
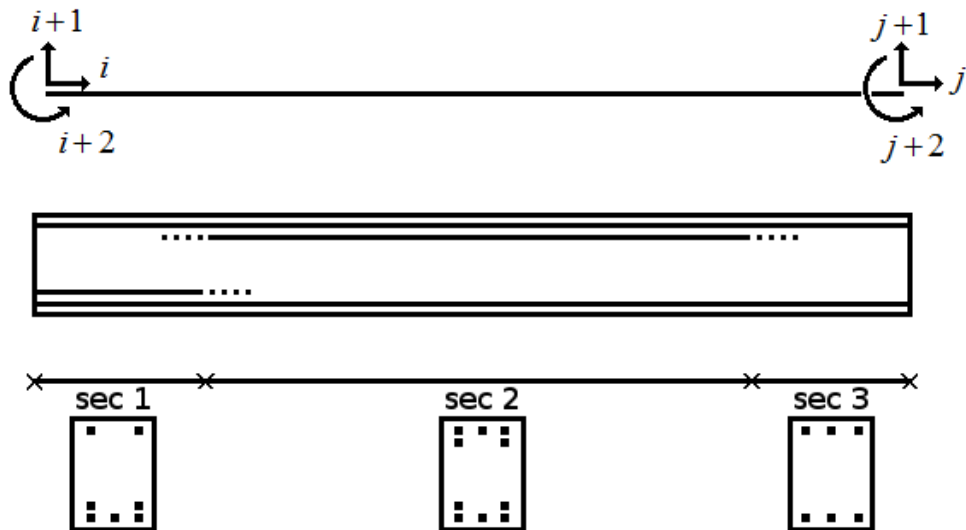
Figure 3.7 Properties of RC member

RC Frame

RC members combine and forms RC frame system. The frame structure holds the member's information and forces applied to degrees of freedom.

3.3 Outline of Solution Algorithm
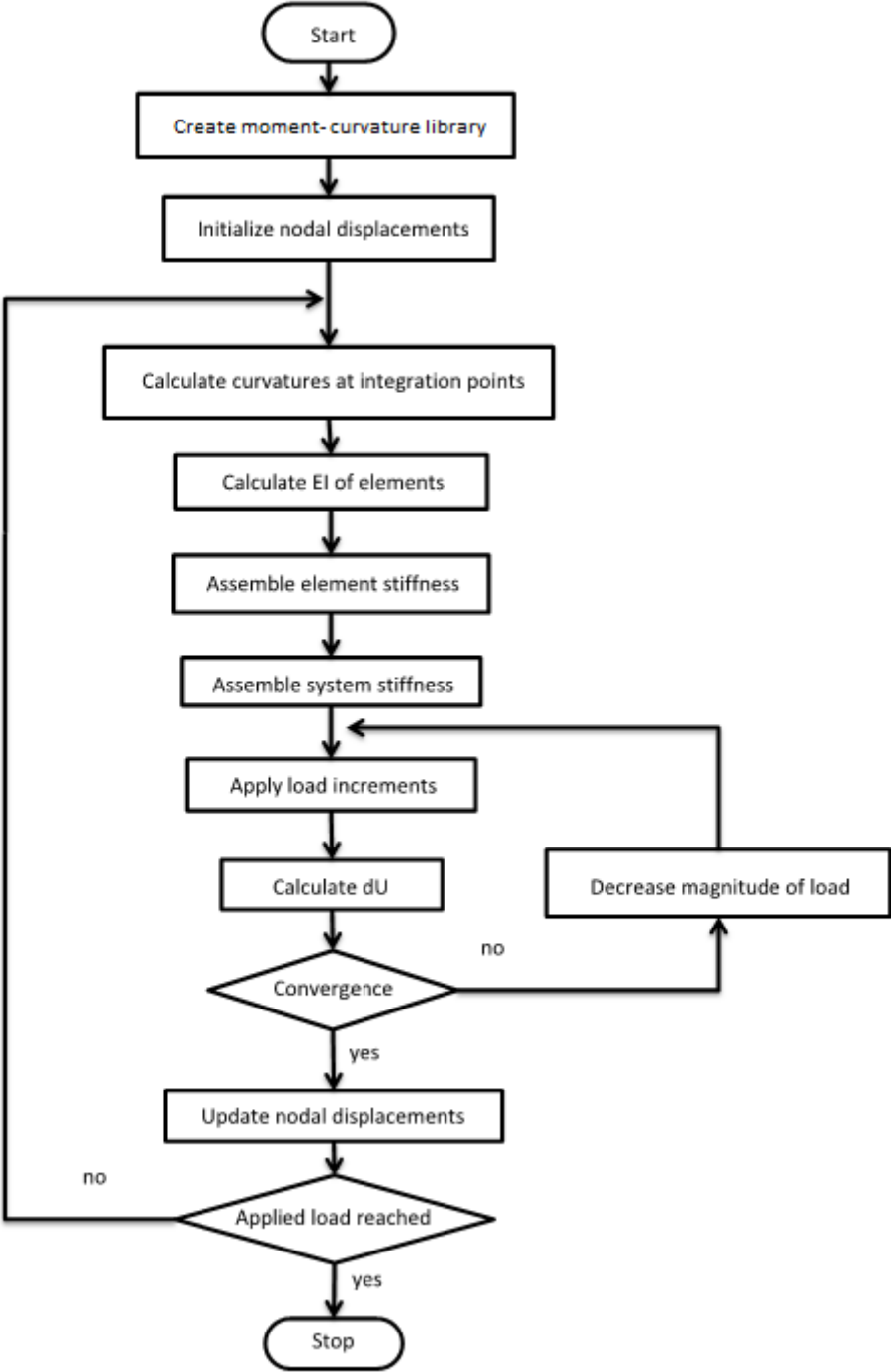
Figure 3.8 Outline of the solution algorithm

The solution algorithm is presented in Figure 3.8. A moment – curvature database is constructed for each section, with varying axial forces. During the analysis the EI parameter is calculated by interpolating the results stored in the database. With this approach the EI parameters calculated once, thus the computation time decreases. The element stiffness is calculated by using the element EI, which is determined by the approximated moment

20

curvature response at each integration point. The system stiffness is assembled by using connectivity information. Then the system is solved for given load increment. If the solution does not converge, the applied load increment divided into two and the iterations continue until convergence. At every increment, the additional displacements are calculated and the system displacements are updated. The stiffness is calculated according to the new displacement field for the next load increment.

CHAPTER 4

VERIFICATION OF ANALYSIS RESULTS

4.1 General

In this chapter, several analysis cases are examined. The purpose of this analysis is to display the different results by changing load conditions, sectional properties and mesh sizes. The load is applied in increasing steps due to the Newton Raphson solution procedure. The results are plotted at each load increment, thus the change of behavior of the element can be seen. If the new increment causes failure, the load increment reduced to its half value until the convergence is obtained.

4.2 Cantilever RC Beam With Point Load (CPL)

4.2.1 Description of the problem

In Figure 4.1, a RC cantilever beam is loaded with a point load at free end. It is modeled with different mesh sizes as 16, 32, 64 and 128.
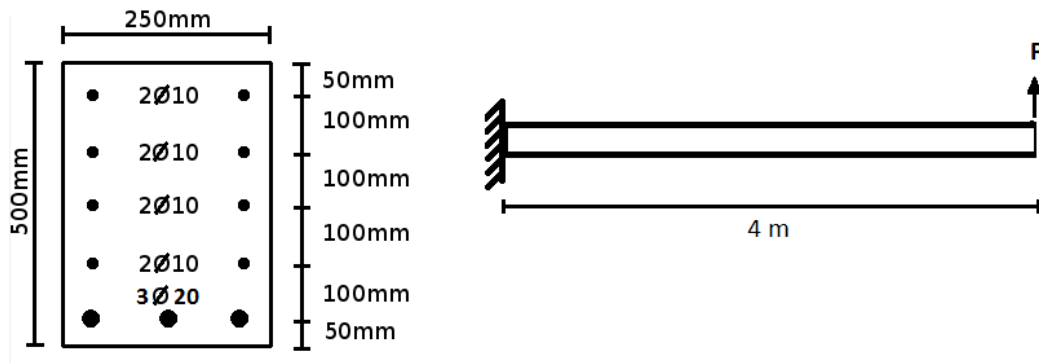
Figure 4.1 Dimensions and section geometry for CPL test case

Concrete and steel material properties:

f_c = 50 MPa $\qquad\qquad\qquad$ f_u = 630 MPa

ε_{co} = 0.0028 $\qquad\qquad\qquad$ ε_{sy} = 0.0021

ε_{cu} = 0.0038 $\qquad\qquad\qquad$ ε_{sh} = 0.0105

f_y = 420 MPa $\qquad\qquad\qquad$ E_s = 200 GP

The concrete model is selected as Hognestad concrete model and the steel model is selected as Kent & Park's steel model.

23

4.2.2 Analysis Results
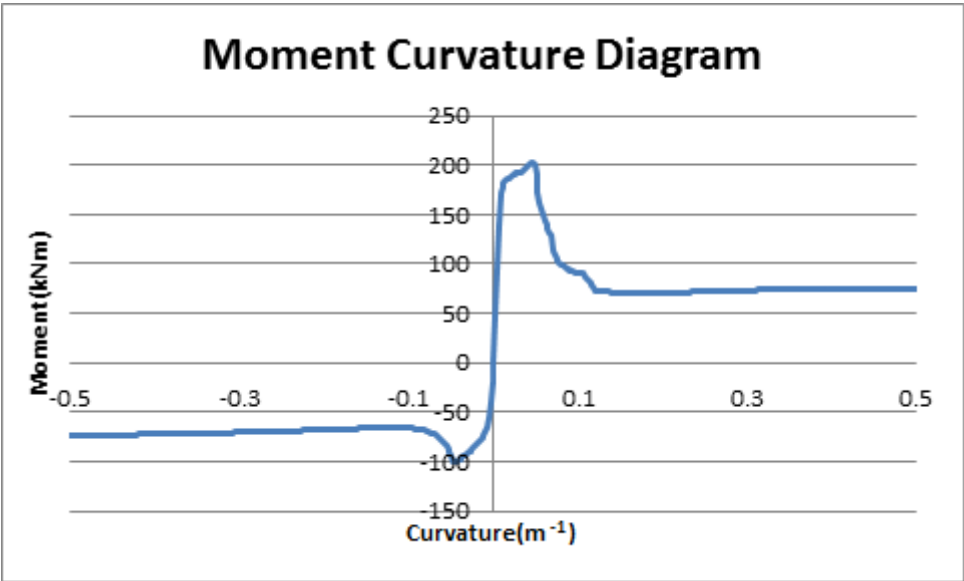
Figure 4.2 Moment curvature diagram of the CPL test case's section

In Figure 4.2, moment curvature diagram of the section is given. The section cannot carry more moment than approximately 200kNm in positive curvature and 100kNm in negative curvature. A section undergoes fiber to fiber redistribution when these moment values are reached. If the curvature of the element is greater than approximately 0.05 m^{-1}, the section capacity reduces to approximately 75kNm, in other words, plastic hinges are formed.
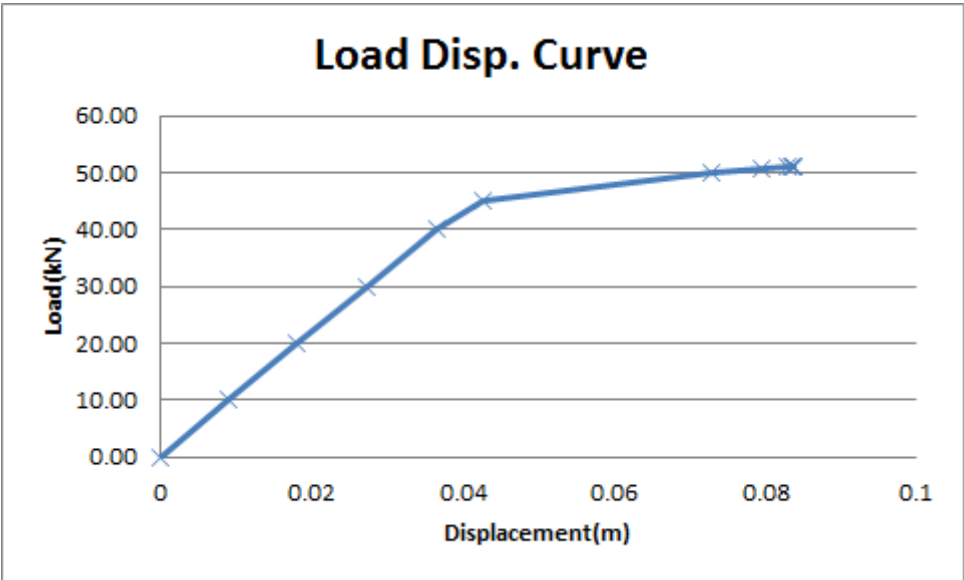
Figure 4.3 Load-Displacement curve for CPL test case for mesh size 128

In Figure 4.3 the load displacement curve is given. Up to 45kN loading the cantilever deformations are in linear range. After 45kN the beam deformation shows nonlinear behavior and plastic hinges are formed. In Figure 4.4, the change of curvatures at integration points is displayed.
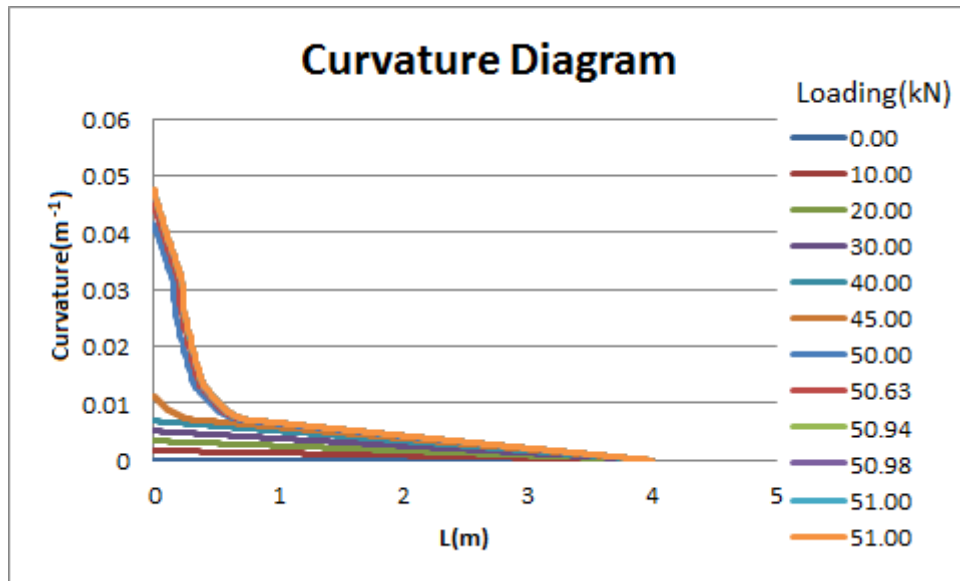
Figure 4.4 Curvature diagram along the member for CPL test case for 128 element mesh
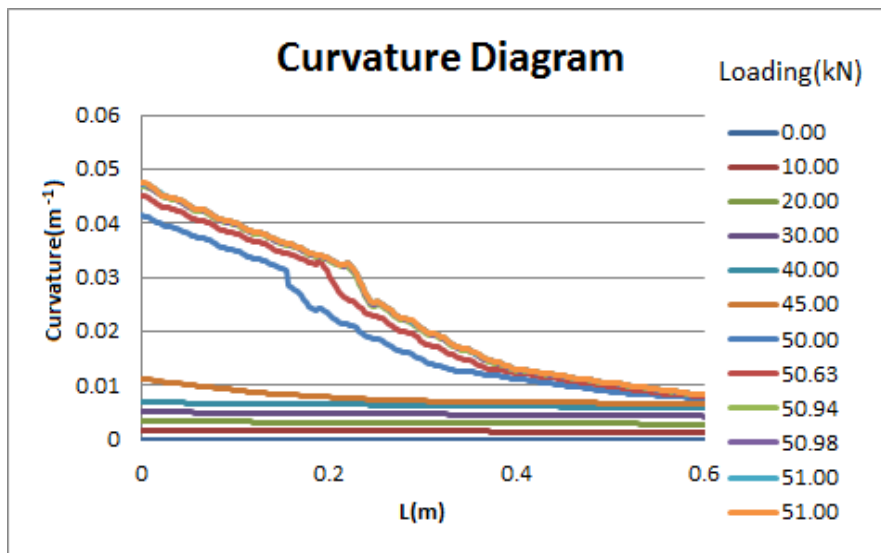
Figure 4.4.a Curvature diagram between 0-0.6 m for CPL test case for 128 element mesh

After 40kN loading, the curvatures at the support zone began to increase. There is a dramatic increase after 50kN loading, followed by a rapid failure. A cantilever beam is a structural element which does not allow formation of mechanisms; thus formation of a plastic hinge results in failure. This is the reason why the moment diagram in Figure 4.5 does not yield before failure. Triangular moment diagram keeps its shape until the failure. The maximum moment in the diagram is approximately 200kNm which is equals to the maximum moment capacity in Figure 4.2.
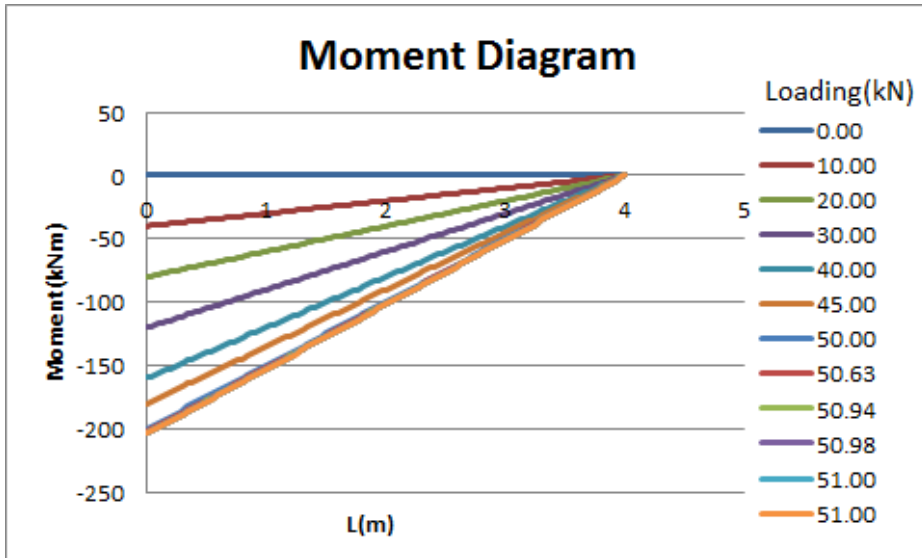
Figure 4.5 Moment diagram of for CPL test case

Table 4.1 Analysis results of CPL test case for different mesh sizes

Mesh Size	Tip Displacement(m)	Allowable Load(kN)	Support Moments(kNm)
16	0.085	51.10	-204.31
32	0.082	51.09	-203.47
64	0.084	51.01	-203.87
128	0.084	51.00	-203.55

In Table 4.1, the tip displacements, support moments and allowable loads are listed according to the varying mesh sizes. As the mesh size increases the support moments are getting closer to the section moment capacity which is 203.1 kNm.
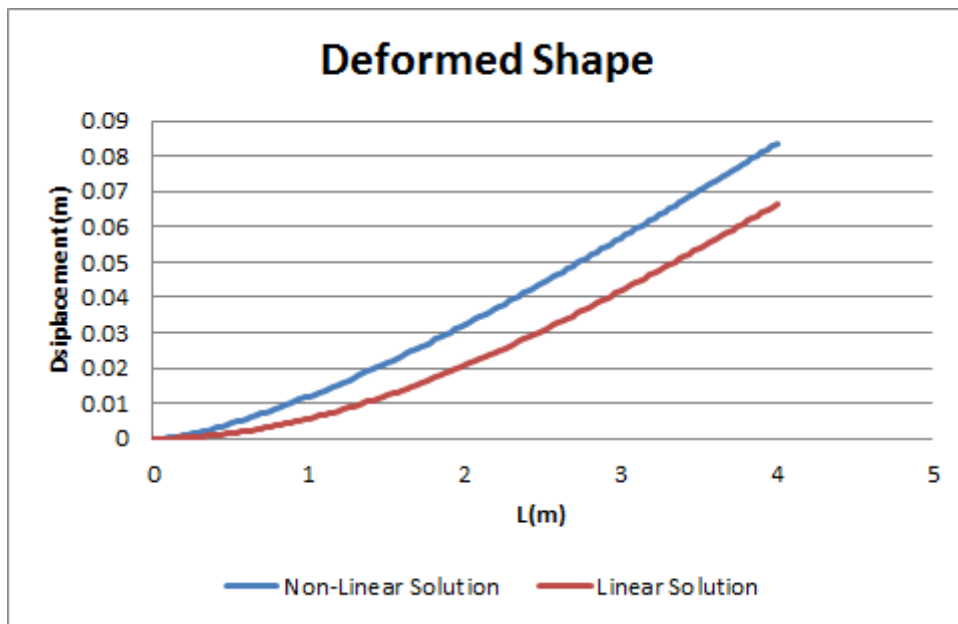
Figure 4.6 Comparison of nonlinear and linear analysis results for CPL test case

26

The deformed shapes of the linear and nonlinear analysis are shown in Figure 4.6. The tip displacement increases due to the nonlinear material behavior. The initial tangent stiffness is used throughout the linear analysis. On the other hand the stiffness of the system is updated at every load increment, thus, the nonlinear analysis results in more refined results in terms of displacements.

4.3 Fixed Supported RC Beam With Point Load (FSPL)

4.3.1 Description of the problem

In Figure 4.7 a fixed supported RC beam is loaded with a point load at mid span. It is modeled with different mesh sizes as 16, 32, 64 and 128.
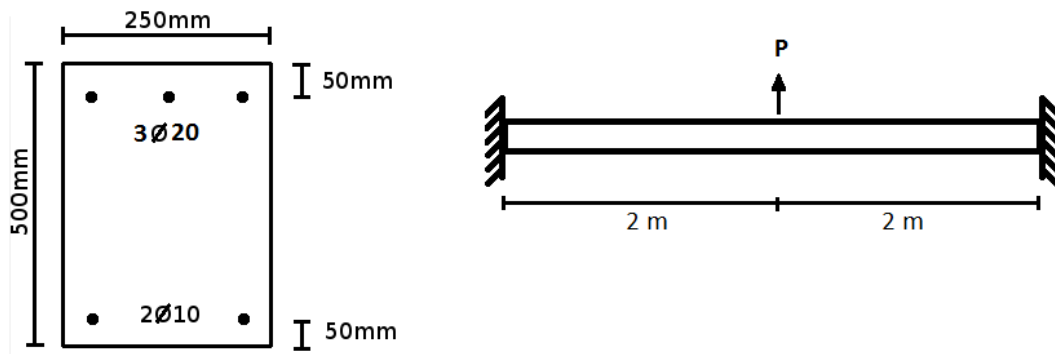
Figure 4.7 Dimensions and section geometry for FSPL test case

Concrete and steel material parameters:

f_c = 50 MPa

ε_{co} = 0.0028

ε_{cu} = 0.0038

ε_{sy} = 0.0021

ε_{sh} = 0.0105

f_y = 420 MPa

f_u = 630 MPa

E_s = 200 GPa

The concrete model is selected as Hognestad concrete model and the steel model is selected as Kent & Park's steel model.

4.3.2 Analysis Results
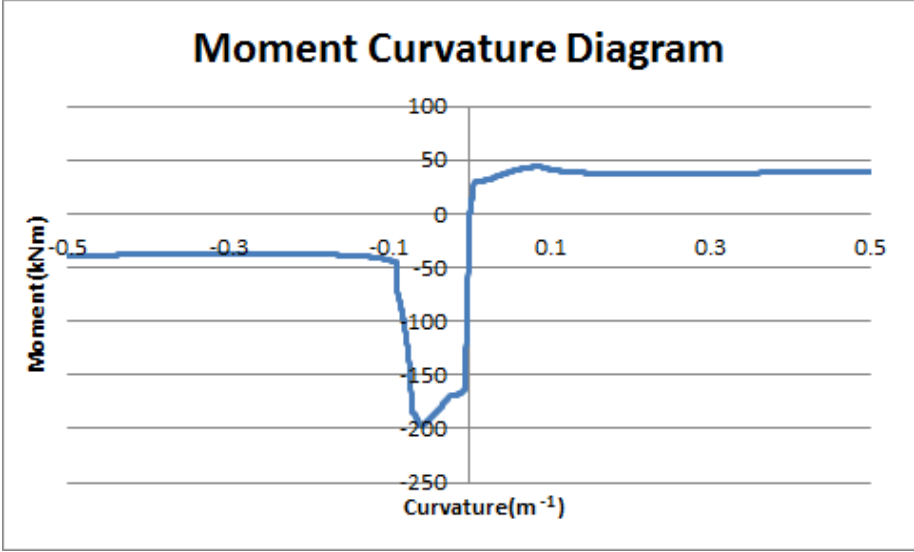
Figure 4.8 Moment curvature diagram of the FSPL test case's section

In Figure 4.8, moment curvature diagram of the section is given. The section cannot carry more moment than approximately 50kNm in positive curvature and 200kNm in negative curvature. A section undergoes fiber to fiber redistribution when these moment values are reached. If the curvature of the element is greater than approximately 0.05, then the section's moment capacity reduces to approximately 45kNm, in other words, plastic hinges are formed.
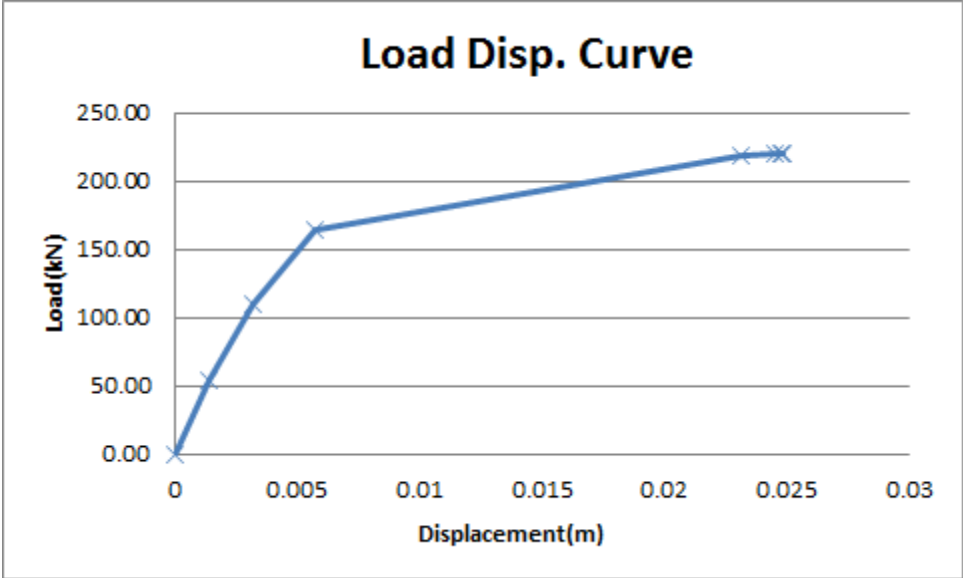
Figure 4.9 Load-Displacement curve for FSPL test case for mesh size 128

In Figure 4.9 the load displacement curve is given for 128 element mesh. Up to 180kN the RC beam deformations are in linear range. After the loading exceeds 180kN the beam deformation shows nonlinear behavior and plastic hinges are formed. In Figure 4.10 the change of curvatures at integration points is displayed.
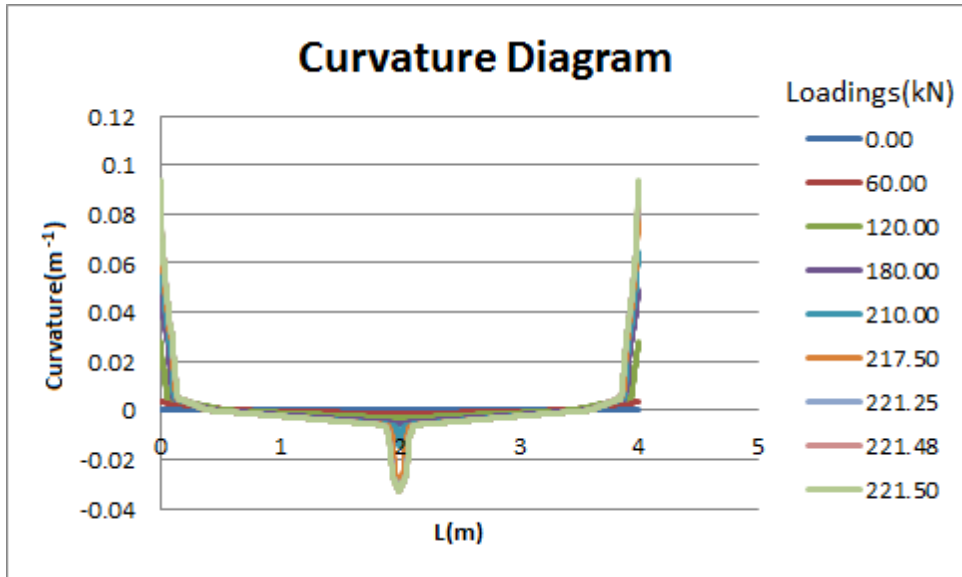
Figure 4.10 Curvature diagram along the member for FSPL test case for 128 element mesh
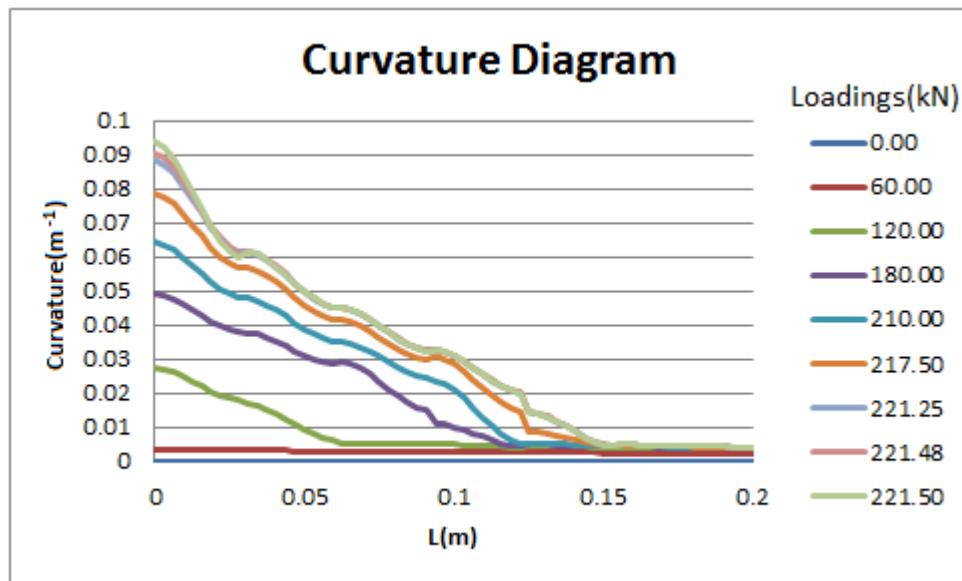
Figure 4.10.a Curvature diagram between 0-0.2 m for FSPL test case for 128 element mesh
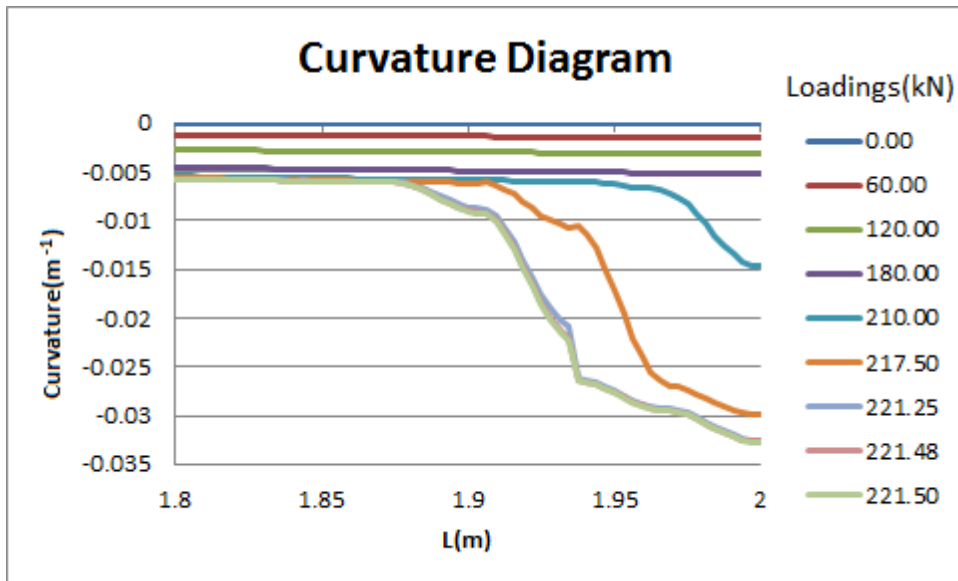
Figure 4.10.b Curvature diagram between 1.8-2.0 m for FSPL test case for 128 element mesh

After 180kN of the applied load, the curvatures at the supports and span zones began to increase. There is a dramatic increase at 240kN loading followed by a rapid failure. Hinges are formed at support and mid span. In Figure 4.11, the change of moment diagram versus load increments is given. During an elastic analysis the inflection points of the moment diagram passes from 1 quarter length away from de supports. But due to the material nonlinearity the inflection points began to move towards to the supports as the load increases.
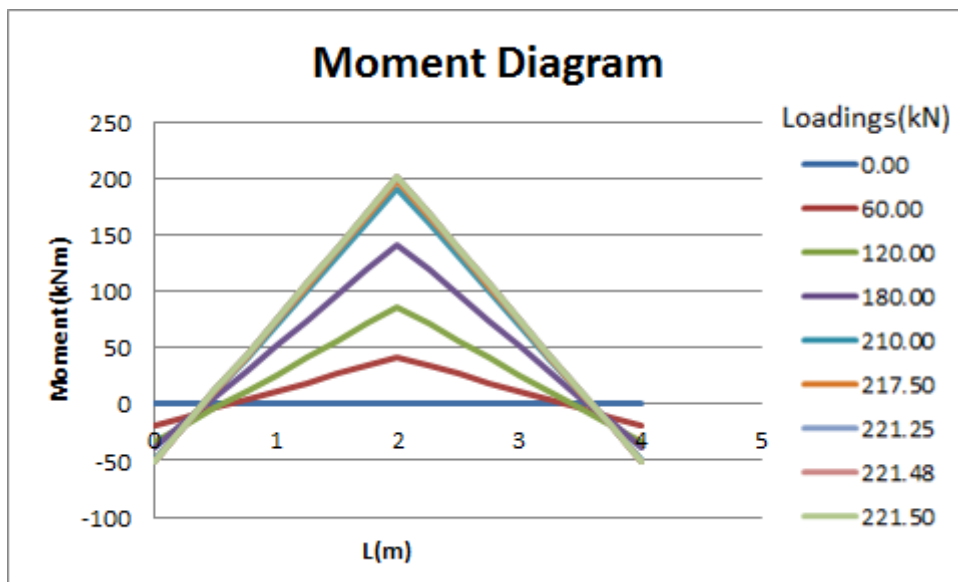
Figure 4.11 Moment diagram of for FSPL test case

In Table 4.2, the tip displacements, support and span moments and allowable loads are listed according to the varying mesh sizes.

Table 4.2 Analysis results of FSPL test case for different mesh sizes

	Mid Span Displacement(m)	Allowable Load(kN)	Support Moment(kNm)	Span Moment(kNm)
16	0.025	251.28	-50.60	200.45
32	0.025	242.23	-43.26	198.78
64	0.024	222.95	-44.89	177.79
128	0.023	221.50	-44.18	176.72
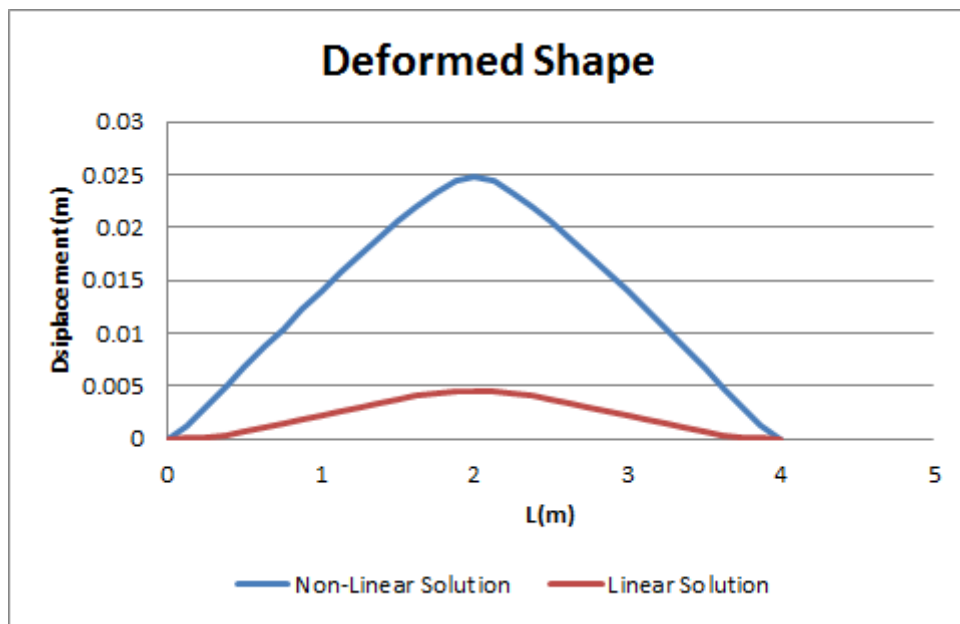
Figure 4.12 Comparison of nonlinear and linear analysis results for FSPL test case

The deformed shapes of the linear and nonlinear analysis are shown in Figure 4.12. The mid span displacement increases due to the nonlinear material behavior. The initial tangent stiffness is used throughout the linear analysis. On the other hand, the stiffness of the system is updated at every load increment thus; the nonlinear analysis is resulted in more slender results in terms of displacements.

Another important result is that the plastic hinges are formed at support and mid span points. The deformed shape resembles a simply supported beam with a hinge at the middle, rather than a fixed end supported beam deformation.

4.4 Cantilever RC Beam With Uniformly Distributed Load (CDL)

4.4.1 Description of the problem

In Figure 4.13, a RC cantilever beam is loaded with a uniformly distributed load through its length. It is modeled with different mesh sizes as 16, 32, 64 and 128.
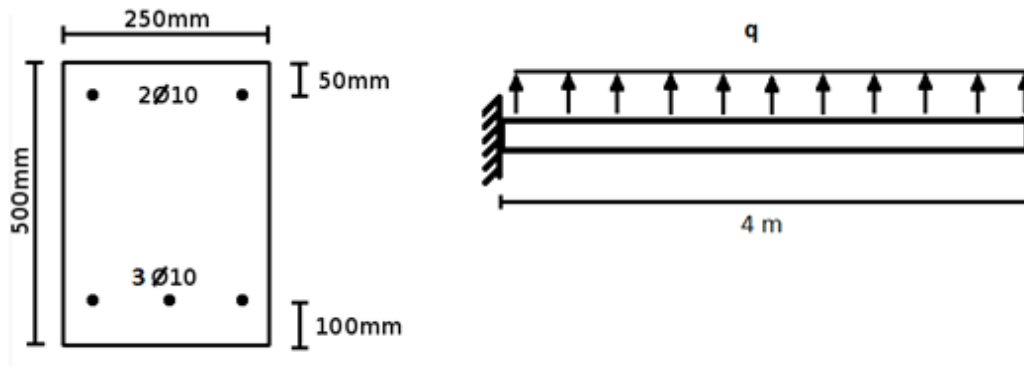
Figure 4.13 Dimensions and section geometry for CDL test case

Concrete and steel material parameters:

f_c = 50 MPa ε_{sh} = 0.0105

ε_{co} = 0.0028 f_y = 420 MPa

ε_{cu} = 0.0038 f_u = 630 MPa

ε_{sy} = 0.0021 E_s = 200 GPa

The concrete model is selected as Hognestad concrete model and the steel model is selected as Kent & Park's steel model.

4.4.2 Analysis Results

Figure 4.14 Moment curvature diagram of the CDL test case's section

In Figure 4.14, moment curvature diagram of the section is given. The section cannot carry more moment than approximately 170kNm in positive curvature and 60kNm in negative curvature. A section undergoes fiber to fiber redistribution when these moment values are reached. If the curvature of the element is greater than approximately 0.06 m^{-1} then the section capacity reduces to approximately 33kNm, in other words, plastic hinges are formed.
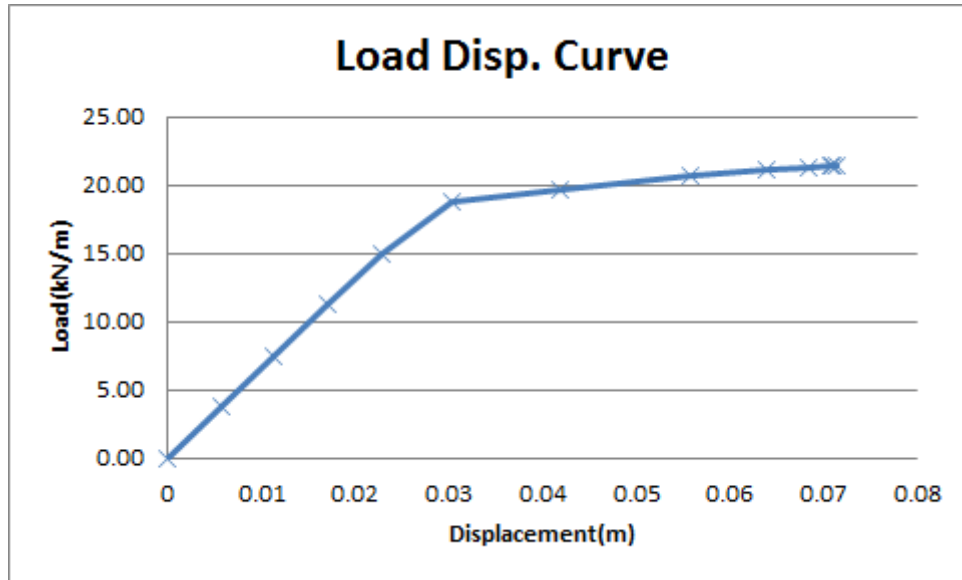
Figure 4.15 Load-Displacement curve for CDL test case for mesh size 128

In Figure 4.15, the load displacement curve is given for the free end of the cantilever beam. Up to 18.75kN/m loading, the cantilever deformations are in linear range. After this limit the beam deformation shows nonlinear behavior and plastic hinges are formed. In Figure 4.16, the change of curvatures at integration points is displayed.
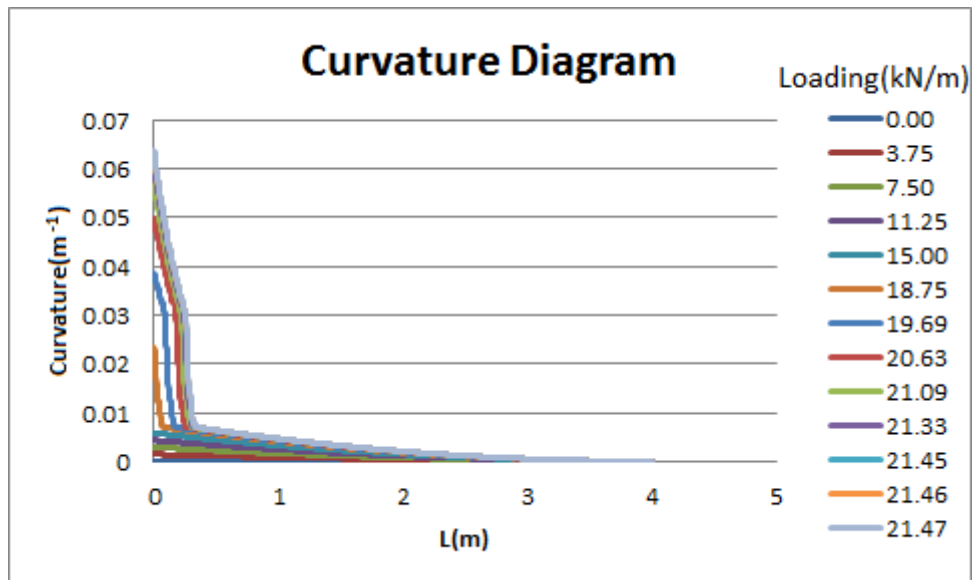
Figure 4.16 Curvature diagram along the member for CDL test case for 128 element mesh
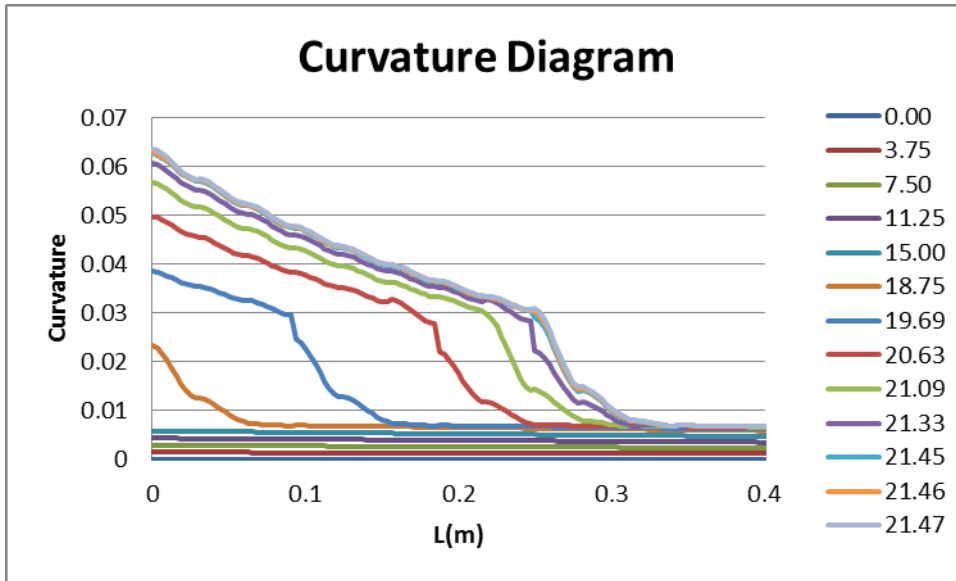
Figure 4.16.a Curvature diagram between 0-0.4 m for CDL test case for 128 element mesh

After application of 15kN/m distributed load, the curvatures at the support zone began to increase. There is a dramatic increase and after 18.75kN/m loading, then followed by a rapid failure. The moment diagram in Figure 4.17 shows that the support moment cannot exceed approximately 170kNm. The moment curvature diagram in Figure 4.13, the maximum moment is approximately 170kNm which is equals to the maximum moment capacity in Figure 4.14.
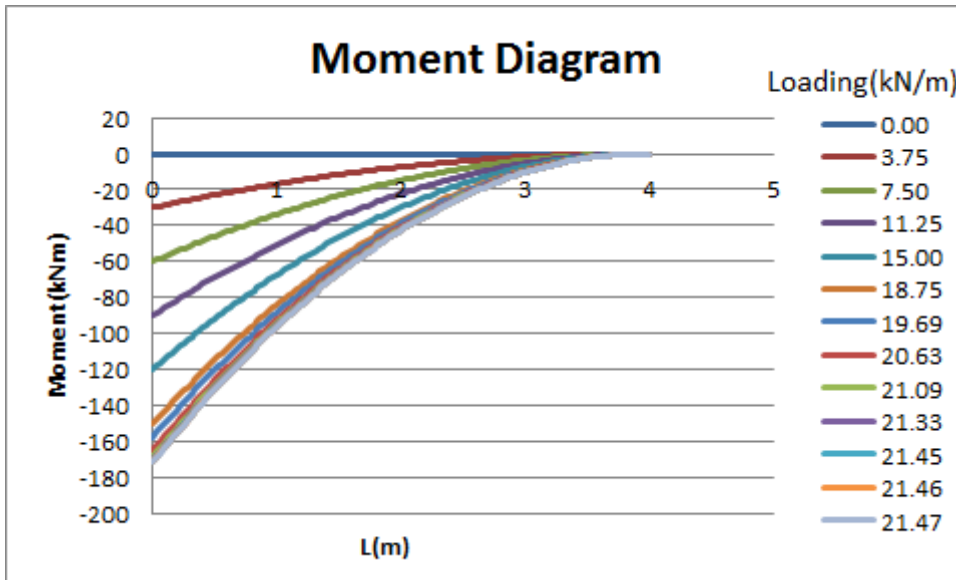
Figure 4.17 Moment diagram of for CDL test case

In Table 4.3 the tip displacements, support moments and allowable loads are listed according to the varying mesh sizes. As the mesh size increases the support moments approaches to the section's moment capacity which is 171.6 kNm. On the other hand the change of tip displacement can be ignored.

Table 4.3 Analysis results of CDL test case for different mesh sizes

Mesh Size	Tip Displacement(m)	Allowable Load(kN/m)	Support Moments(kNm)
16	0.072	21.69	-173.44
32	0.072	21.54	-172.21
64	0.071	21.49	-171.79
128	0.071	21.47	-171.61
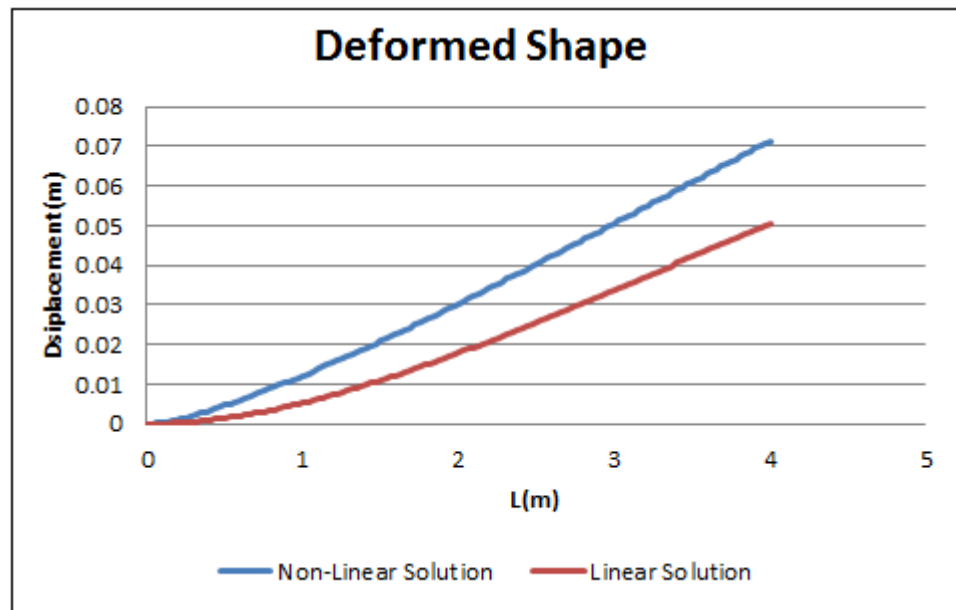
Figure 4.18 Comparison of nonlinear and linear analysis results for CDL test case

The deformed shapes of the linear and nonlinear analysis are shown in Figure 4.18. The displacement of the free end increases due to the nonlinear material behavior. The initial tangent stiffness is used throughout the linear analysis. On the other hand, the stiffness of the system is updated at every load increment step, thus, the nonlinear analysis is resulted in more slender results in terms of displacements. Due to the plastic hinging at the supports, the displaced shape is closer to a straight beam rather than a deformed cantilever.

4.5 Fixed Supported RC Beam With Uniformly Distributed Load (FSDL)

4.5.1 Description of the problem

In Figure 4.19, a RC fixed supported beam is loaded with a uniformly distributed load through its length. It is modeled with different mesh sizes as 16, 32, 64 and 128.
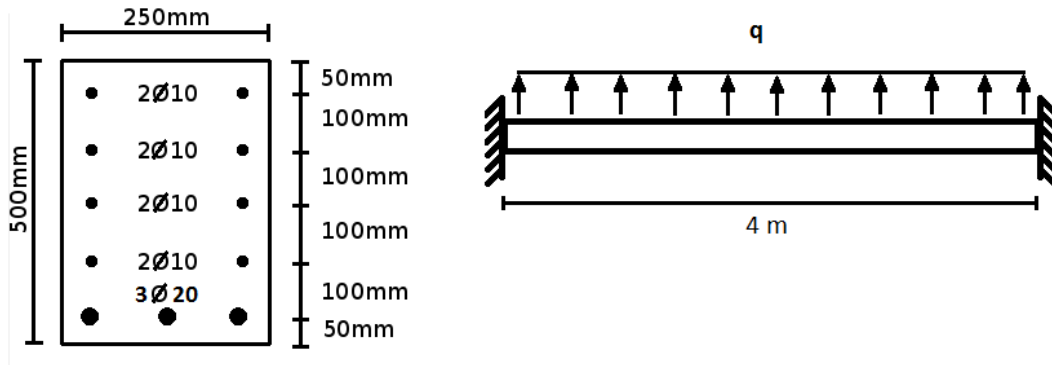
Figure 4.19 Dimensions and section geometry for FSDL test case

Concrete and steel material parameters:

$f_c = 50$ MPa

$\varepsilon_{sh} = 0.0105$

$\varepsilon_{co} = 0.0028$

$f_y = 420$ MPa

$\varepsilon_{cu} = 0.0038$

$f_u = 630$ MPa

$\varepsilon_{sy} = 0.0021$

$E_s = 200$ GPa

The concrete model is selected as Hognestad concrete model and the steel model is selected as Kent & Park's steel model.
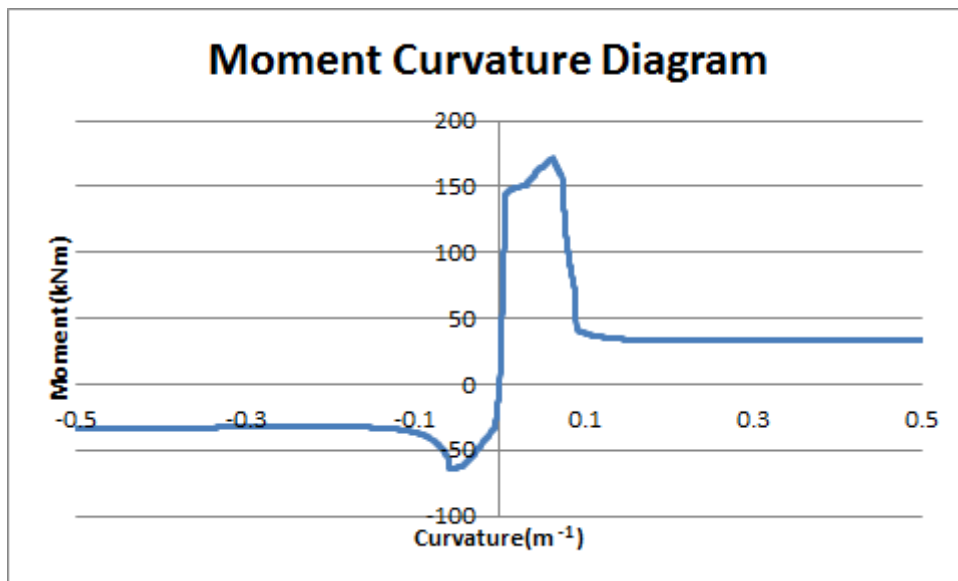
4.5.2 Analysis Results

Figure 4.20 Moment curvature diagram of the FSDL test case's section

In Figure 4.20, moment curvature diagram of the section is given. The section cannot carry more moment than approximately 200kNm in positive curvature and 100kNm in negative curvatures. This section undergoes fiber to fiber redistribution when these moment values are reached. If the curvature of the element is greater than approximately 0.05 m^{-1}, then the section capacity reduces to approximately 70kNm, in other words, plastic hinges are formed.
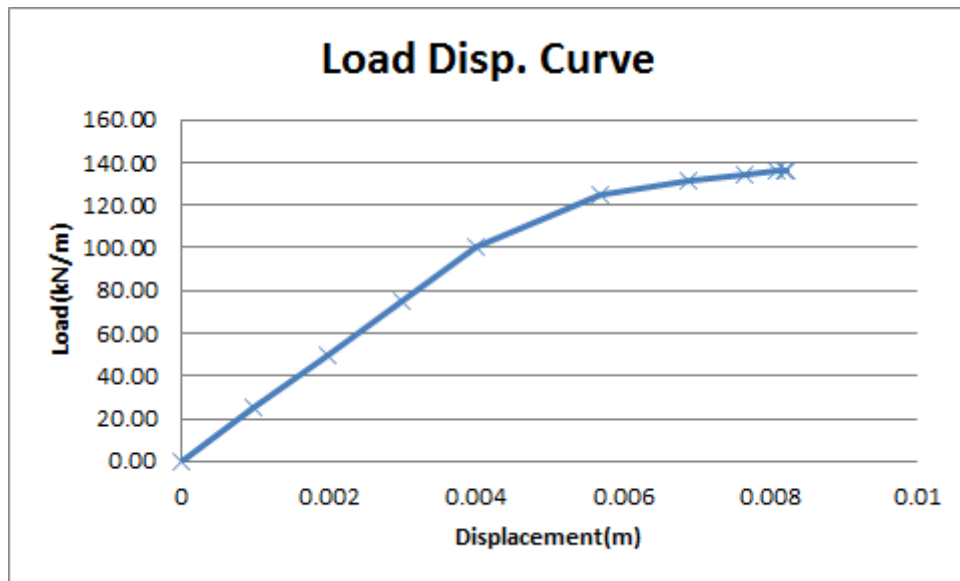
Figure 4.21 Load-Displacement curve for FSDL test case for mesh size 128

In Figure 4.21, the load displacement curve is given for the mid span of the fixed supported beam. Up to 100kN/m loading, the beam deformations are in linear range. After this limit, the beam deformation shows nonlinear behavior and plastic hinges are formed. In Figure 4.22, the change of curvatures at integration points is displayed.
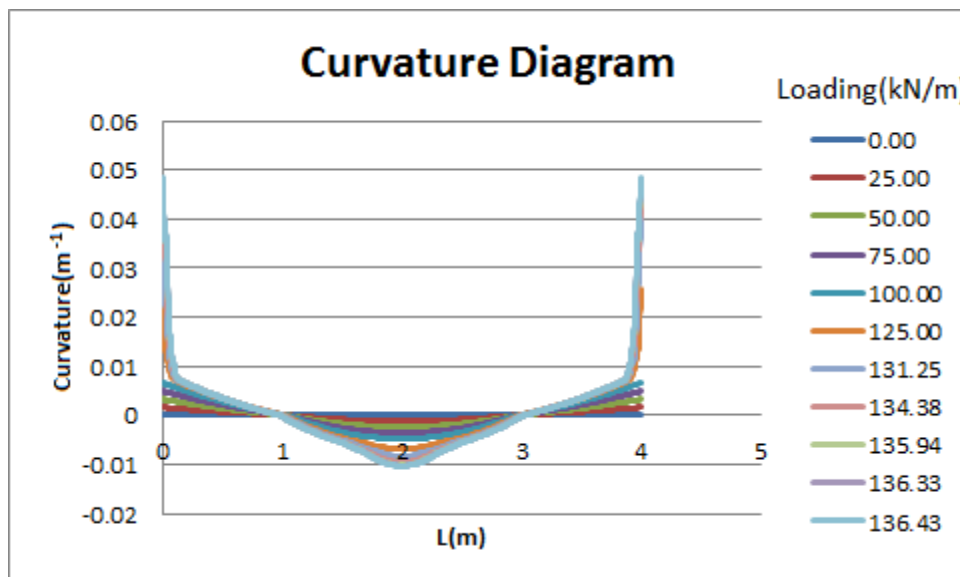
Figure 4.22 Curvature diagram along the member for FSDL test case for 128 element mesh
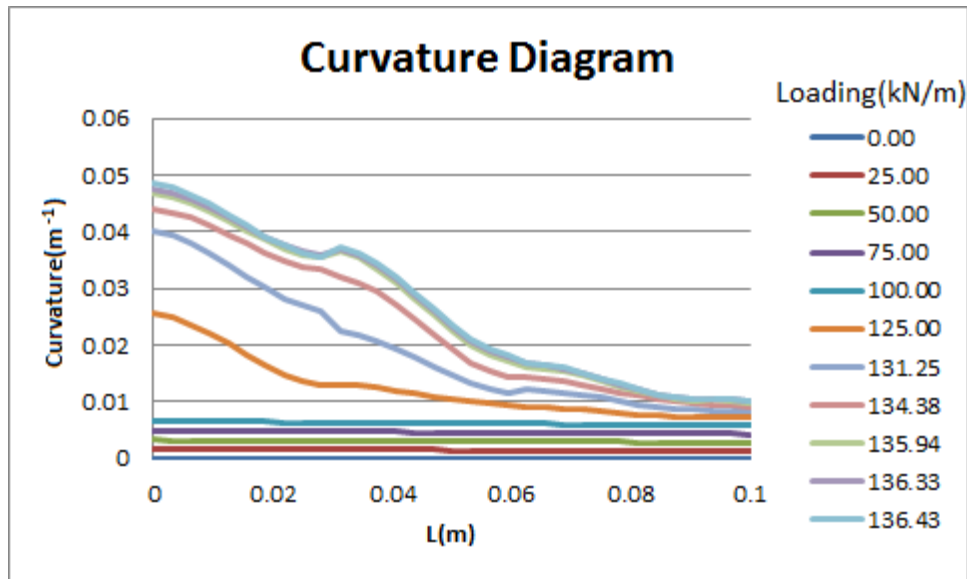
Figure 4.22.a Curvature diagram between 0-0.6 m for FSDL test case for 128 element mesh

After 100kN/m loading, the curvatures at the support zones began to increase. There is a dramatic increase and after 125kN/m loading, then followed by a rapid failure. The moment diagram in Figure 4.20 shows that the support moment cannot exceed approximately 200kNm. The moment curvature diagram in Figure 4.22, the maximum moment in the diagram is approximately 200kNm. That is the same value as the maximum moment capacity in Figure 4.23.
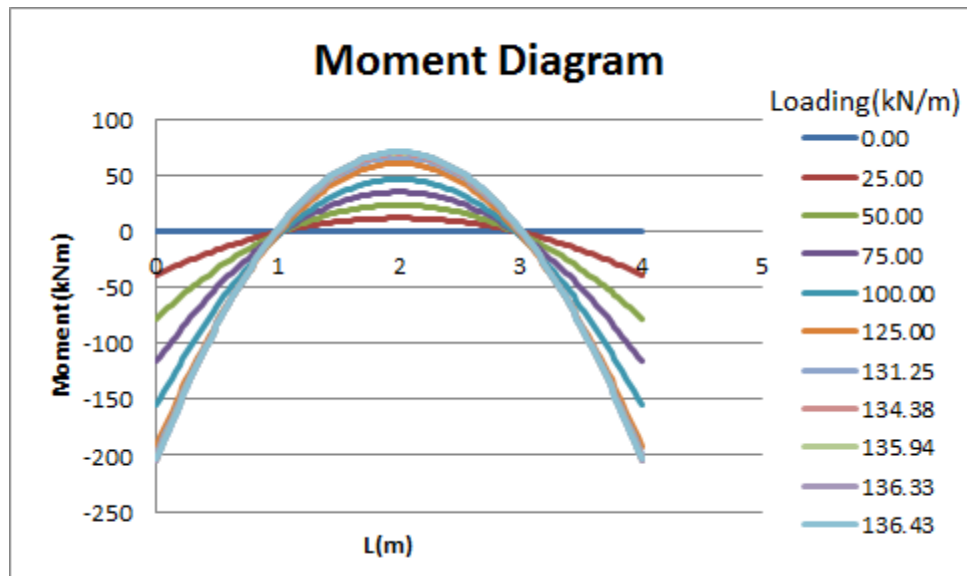
Figure 4.23 Moment diagram of for FSDL test case

In Table 4.4, the tip displacements, support moments and allowable loads are listed according to the varying mesh sizes. The moment capacity of the section is 203.11 kNm. For low mesh sizes such as 16 and 32, the support moments are higher than the section capacity. As the mesh size increases the support moments approaches to 203.11 kNm. The 64 element mesh element fails before the section capacity is reached. This may be caused because of a numerical error. The tip deflection is lower than the 128 element meshed model's deflection meaning that it fails prematurely.

38

Table 4.4 Analysis results of FSDL test case for different mesh sizes

| Mesh Size	Mid Span Displacement(m)	Allowable Load(kN/m)	Support Moments(kNm)
16	0.0130	140.08	-217.07
32	0.0092	135.74	-206.20
64	0.0080	134.47	-201.76
128	0.0082	136.43	-203.28
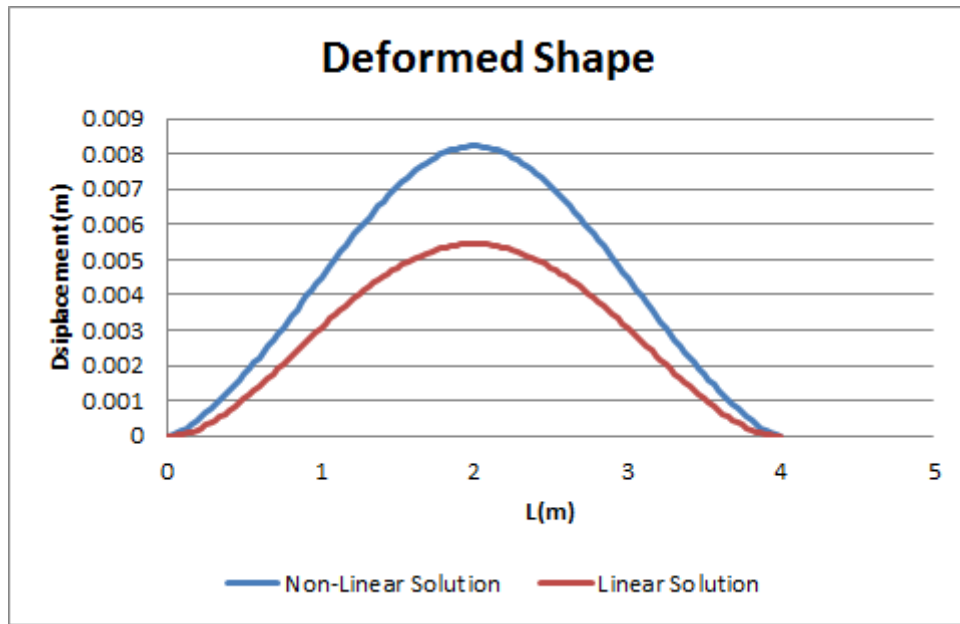
Figure 4.24 Comparison of nonlinear and linear analysis results for FSDL test case

The deformed shapes of the linear and nonlinear analysis are shown in Figure 4.24. The mid span displacement increases due to the nonlinear material behavior. The initial tangent slope of the moment curvature diagram is used throughout the linear analysis as EI of the section. On the other hand the stiffness of the system is updated at every load increment thus the nonlinear analysis is resulted in more slender results in terms of displacements. Due to the softening of the system stiffness the displacements increase nearly 60% with respect to the linear analysis.

4.6 Fixed Supported RC Beam With Uniformly Distributed Load with Axial Compression (FSDLA)

4.6.1 Description of the problem

In Figure 4.19, a RC fixed supported beam, which is loaded with a uniformly distributed load through its length, is shown. It is modeled with different mesh sizes as 16, 32, 64 and 128.

Figure 4.25 Dimensions and section geometry for FSDLA test case

Concrete and steel material parameters:

f_c = 50 MPa

ε_{co} = 0.0028

ε_{cu} = 0.0038

ε_{sy} = 0.0021

ε_{sh} = 0.0105

f_y = 420 MPa

f_u = 630 MPa

E_s = 200 GPa

The concrete model is selected as Hognestad concrete model and the steel model is selected as Kent & Park's steel model.
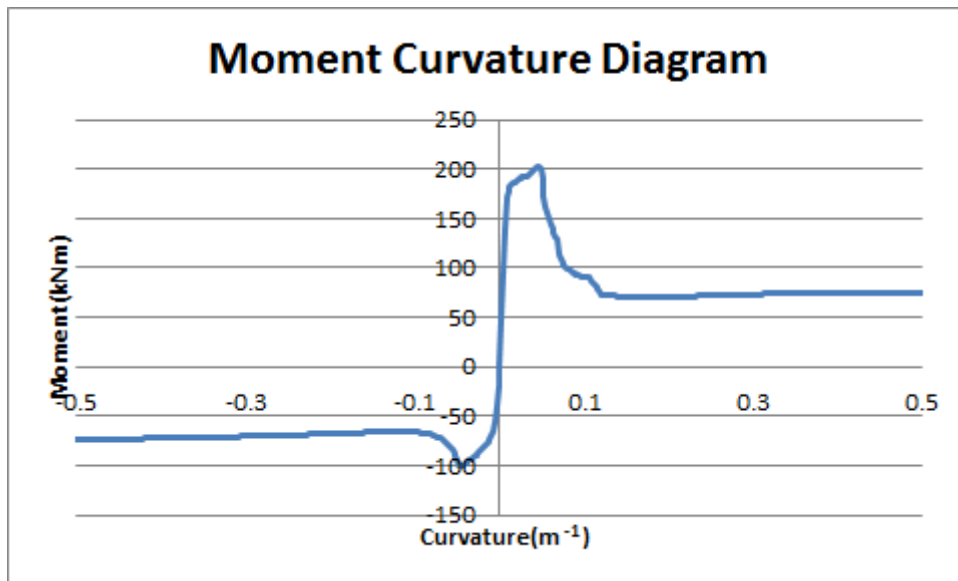
4.6.2   Analysis Results

.
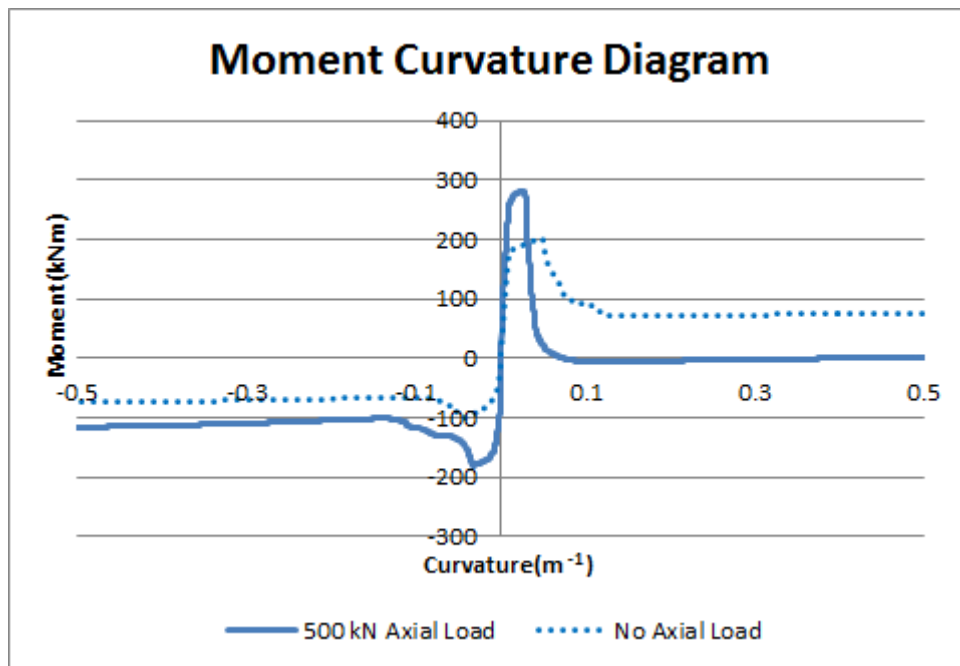
Figure 4.26 Moment curvature diagram of the FSDLA test case's section

In Figure 4.26, moment curvature diagram of the section is given. The compressive axial load increases both positive and negative moment capacities however; it also decreases the ductility of the element. This section cannot carry more moment than approximately 280kNm in positive curvature and 180kNm in negative curvatures. This section undergoes fiber to fiber redistribution when these moment values are reached. If the curvature of the element is greater than approximately 0.03 m^{-1}, the plastic hinges are formed.
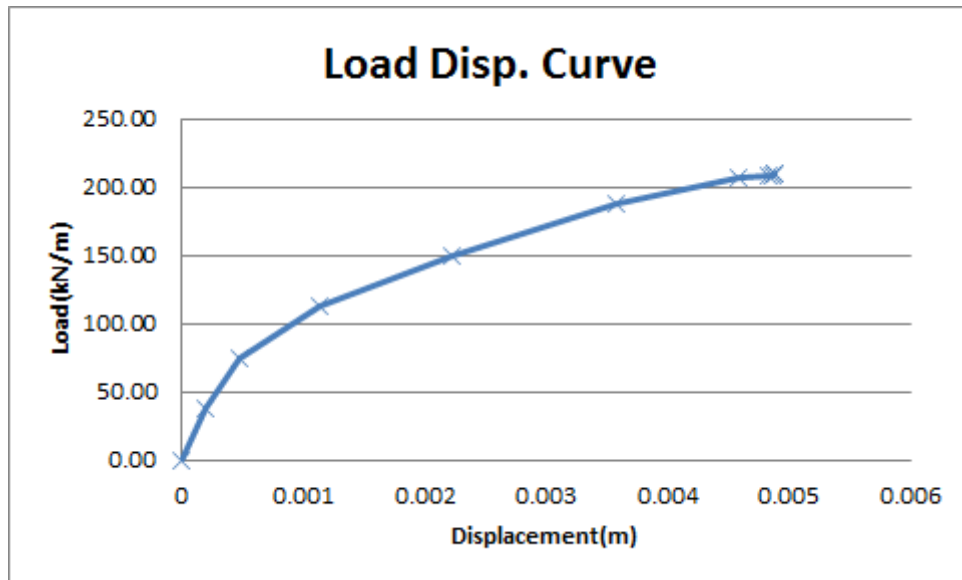
Figure 4.27 Load-Displacement curve for FSDLA test case for mesh size 128

In Figure 4.27, the load displacement curve is given for the mid span of the fixed supported beam. Up to 75kN/m loading, the beam deformations are in linear range. After this limit, the beam deformation shows nonlinear behavior and plastic hinges are formed. In Figure 4.22, the change of curvatures at integration points is displayed.
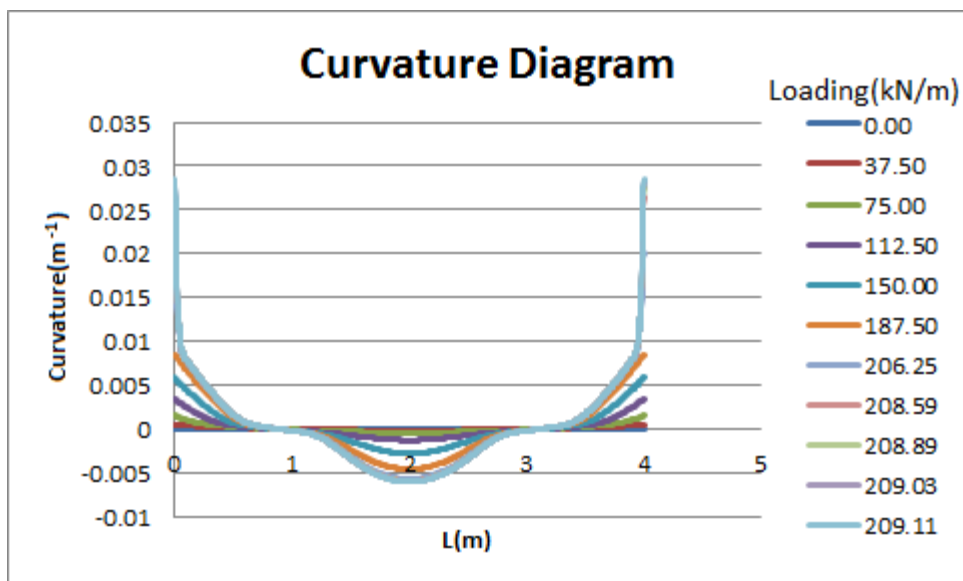
Figure 4.28 Curvature diagram along the member for FSDLA test case for 128 element mesh
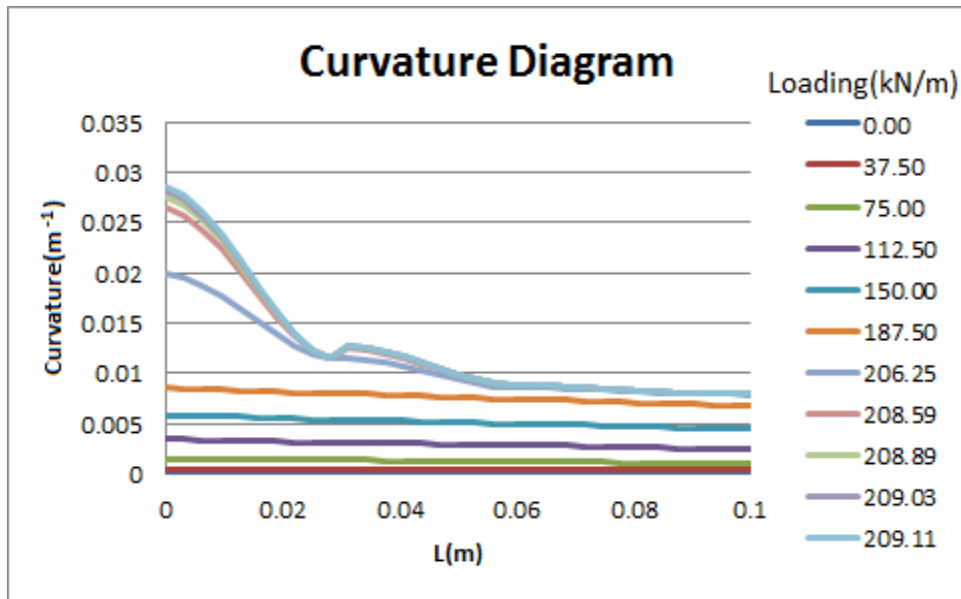
Figure 4.28.a Curvature diagram between 0-0.1 m for FSDLA test case for 128 element mesh

After 75kN/m loading, the curvatures at the support zone began to increase. There is a dramatic increase and after 209kN/m distributed loading and further loading causes failure. The curvatures at the support points increase by 200%. The moment diagram in Figure 4.29 shows that the support moment cannot exceed approximately 300kNm. At the moment curvature diagram in Figure 4.29, the maximum moment is approximately 300kNm, which is equals to the maximum moment capacity in Figure 4.26.
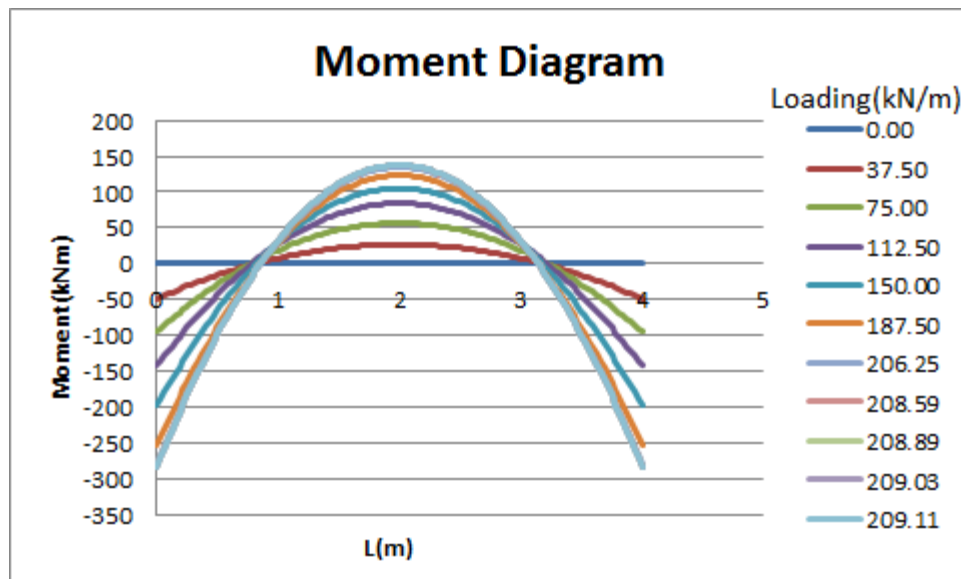
Figure 4.29 Moment diagram of for FSDLA test case
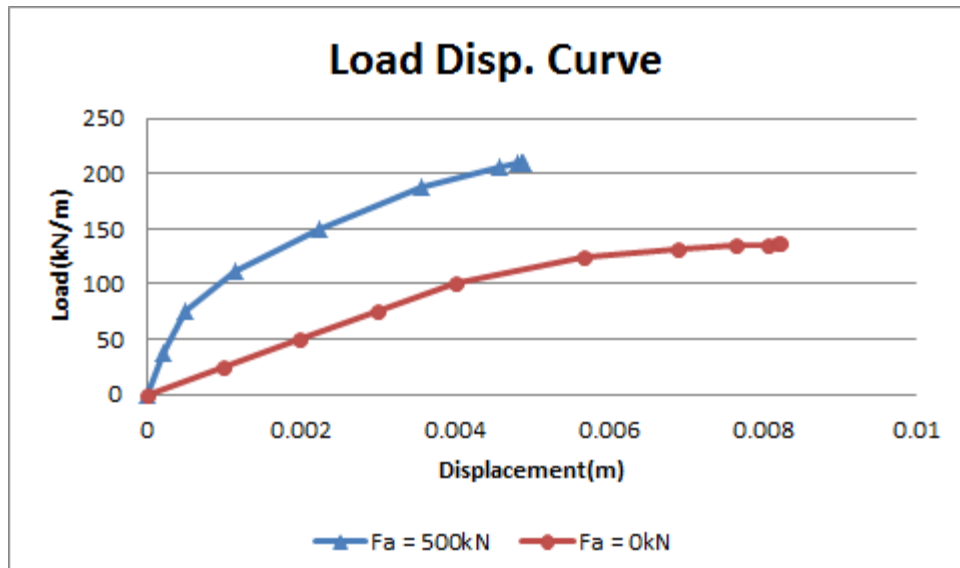
Figure 4.30 Effect of axial compression for FSDL test case

In Figure 4.30 the load-displacement curves of the same beam, with and without compression, are compared. When axial force is applied the member can carry more loads. On the other hand it shows less displacement, in other words, it loses its ductility.

In Table 4.5 the tip displacements, support moments and allowable loads are listed according to the varying mesh sizes.

Table 4.5 Analysis results of FSDLA test case for different mesh sizes

Mesh Size	Mid Span Displacement(m)	Allowable Load(kN/m)	Support Moments(kNm)
16	0.008	220.17	-309.83
32	0.006	214.56	-294.16
64	0.005	210.64	-286.44
128	0.005	209.11	-283.11

According to the Table 4.5, the mid span deflections are higher than the expected when a low density mesh is used. The section capacity of the element's section is 281.20 kNm according to the moment curvature diagram. The 16 element mesh has higher internal forces than its capacity and also has higher span deflection. As the mesh density increases the internal forces converges to the section capacity. Also the span deflection converges to 5 mm.

4.7 Simply Supported Beam with Point Load (SSPL1)

4.7.1 Description of the problem

In Figure 4.31, a RC simply supported beam, which is loaded with two point loads at equal lengths from supports, is shown. It is the same beam configuration with the T1MA beam, tested in the article of Kwak, H.G and Kim, S,P. Nonlinear Analysis of RC Beams Based on Moment-Curvature Relation.
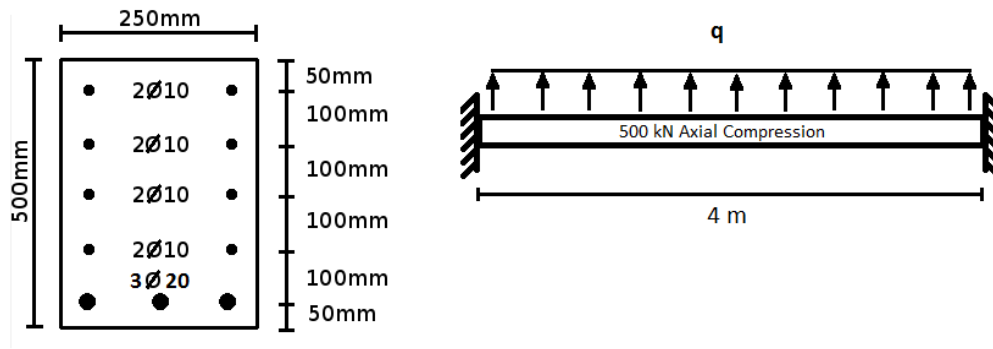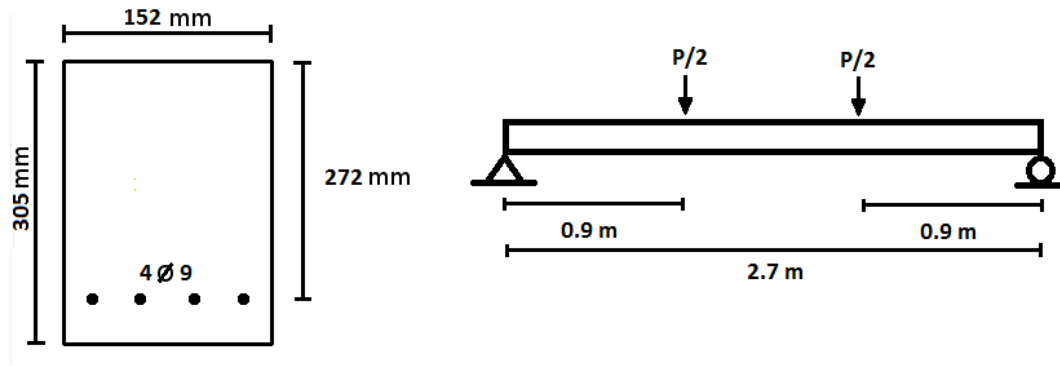
Figure 4.31 Dimensions and section geometry for SSPL1 test case

Concrete and steel material parameters:

f_c = 31.7 MPa

ε_{co} = 0.002

ε_{cu} = 0.003

ε_{sy} = 0.00163

ε_{sh} = 0.00817

f_y = 317 MPa

E_s = 194 GPa

4.7.2   Analysis Results
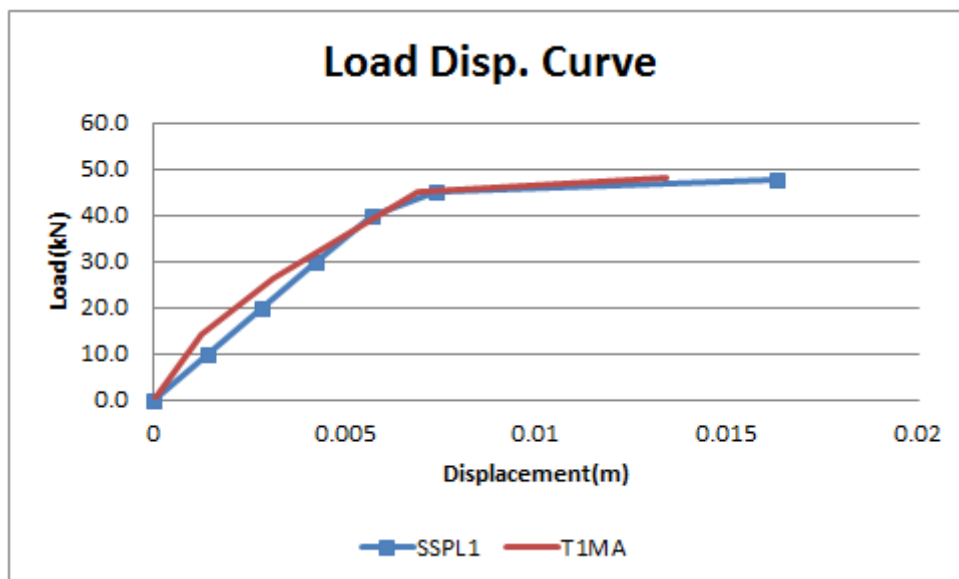
Figure 4.32 Span deflections of SSPL1 and T1MA

T1MA and SSPL1 display similar behavior both in linear deformation range and yielding point. The T1MA beam fails before the calculated displacement in the SSPL1 analysis. The reinforcing bars are assumed to be perfectly bonded to the concrete during the analysis. But in the real life situation, as the concrete cracks, the bond between reinforcing bar and the concrete weakens. In major cracks, the tension steel slips inside the concrete allowing more displacements. Both T1MA and the SSPL1 beams yield at 45 kN loading and their initial stiffness are close to each other.

44

4.8 Simply Supported Beam with Point Load (SSPL2)

4.8.1 Description of the problem

In Figure 4.33, a RC simply supported beam, which is loaded with a single point loads at mid span, is shown. It is the same beam configuration with the J4 beam, tested in the article of Kwak, H.G and Kim, S,P. Nonlinear Analysis of RC Beams Based on Moment-Curvature Relation.
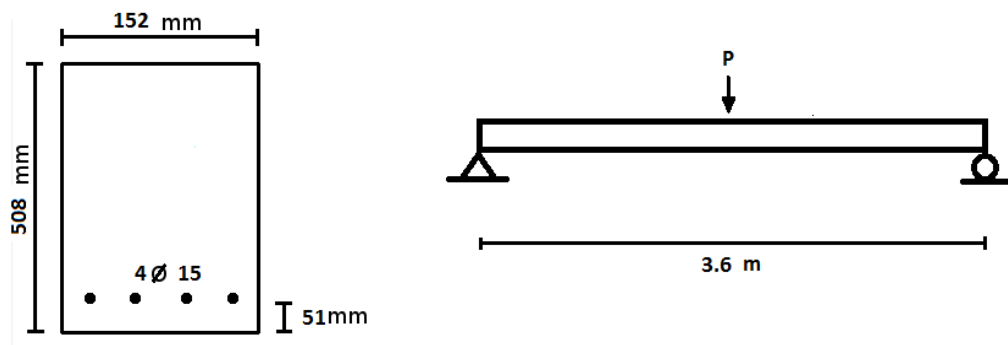
Figure 4.33 Dimensions and section geometry for SSPL2 test case

Concrete and steel material parameters:

f_c = 33.3MPa

ε_{co} = 0.002

ε_{cu} = 0.003

ε_{sy} = 0.00153

ε_{sh} = 0.00763

f_y = 309.6 MPa

E_s = 202.1 GPa

4.8.2 Analysis Results
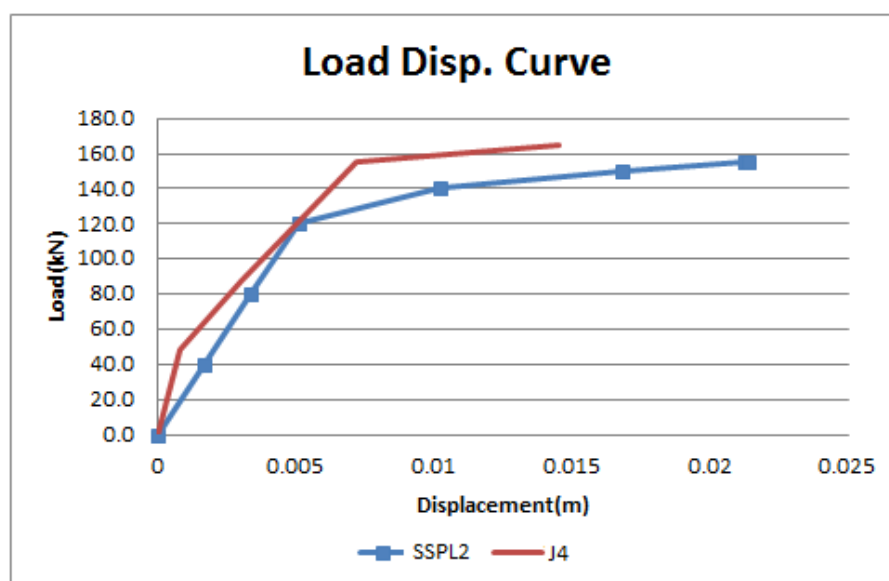
Figure 4.34 Span deflections of SSPL2 and J4

45

SSPL2 beam displays similar behavior to the J4 beam, but the results are not as close as at the SSPL1 and T1MA. SSPL2 beam displays linear deformation up to 120 kN of loading. On the other hand, the J4 beam is stiffer than the SSPL2 up to 50 kN of loading and then it starts a gradual yielding. The SSPL2 beam experiences a sharp transition from linear region to yielding region. The calculated load carrying capacity of the beam is lower than the actual capacity. The J4 beam fails before SSPL2 beam. Due to the bond slip effect, the J4 beam fails at 0.015 m displacement whereas, the SSPL2 beam deforms more due to the perfect bonding between reinforcement and concrete assumption.

4.9 Frame Analysis (FA)

4.9.1   Description of the problem

In Figure 4.35, a RC frame system is shown. It consists of two identical columns and a beam.
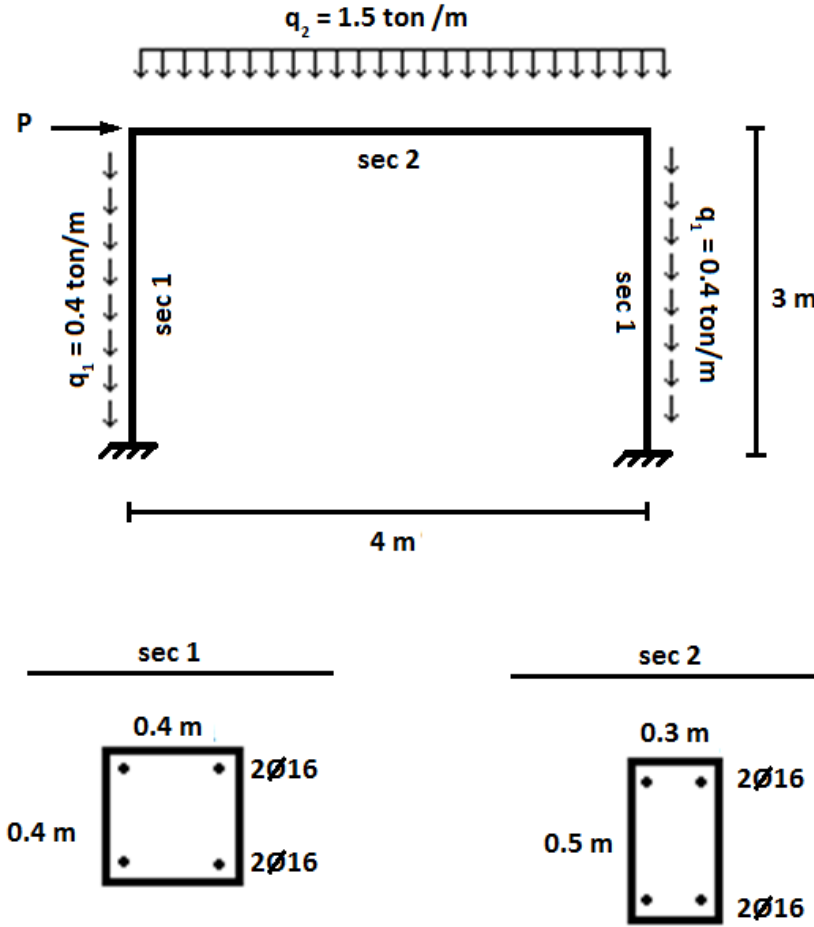
Figure 4.35 Dimensions and section geometries for FA test case

Concrete and steel material parameters:

f_c = 20 MPa $\qquad\qquad\qquad\qquad\qquad$ ε_{sh} = 0.0105

ε_{co} = 0.002 $\qquad\qquad\qquad\qquad\qquad$ f_y = 420 MPa

ε_{cu} = 0.003 $\qquad\qquad\qquad\qquad\qquad$ E_s = 200 GPa

ε_{sy} = 0.0021 $\qquad\qquad\qquad\qquad\qquad$ Clear cover = 5 cm

The analysis consists of two stages; the dead load stage and the lateral load stage. The first stage is the application of dead load. The unit weight of concrete is taken as 2.4 tons / m³. The columns carry only their weights as a uniformly distributed load. On the other hand, the beam carries both itself and the load transferred from the slab. This is why q2 is greater than q1. Due to the axial loading on columns, the ductility of the columns is reduced. In other words, they carry more loads, but become brittle. The gravitational loads are applied in 10 increments. Due to the magnitude of the loading, the deformations are small and in the linear range. It is clear that under dead load, the structures should not display nonlinear behavior. The second part is the application of lateral load, P. The load is applied until the frame fails. In Figure 4.36 and Figure 4.37, the deformed shapes of first and second stages are displayed.

4.9.2 Analysis Results
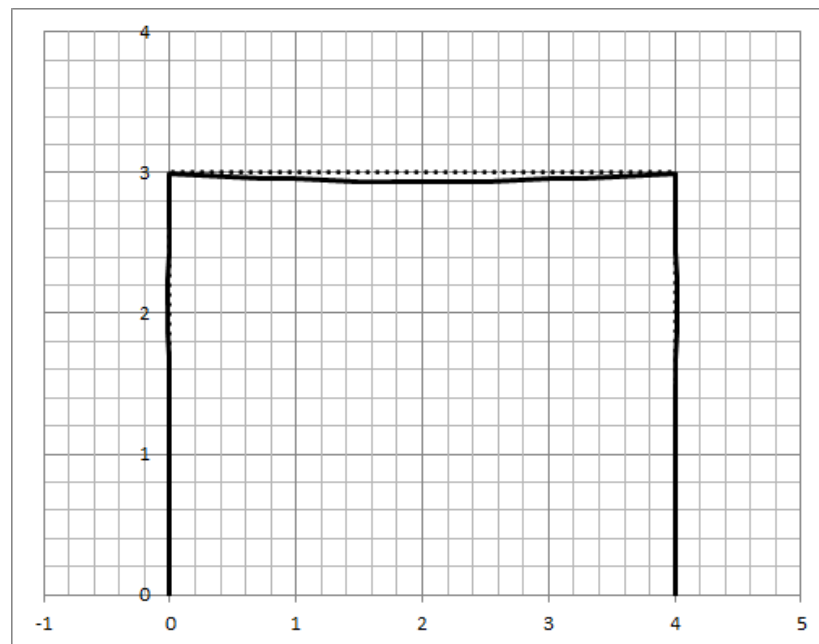
Figure 4.36 Deformed shape under dead loads (magnified 100 times)
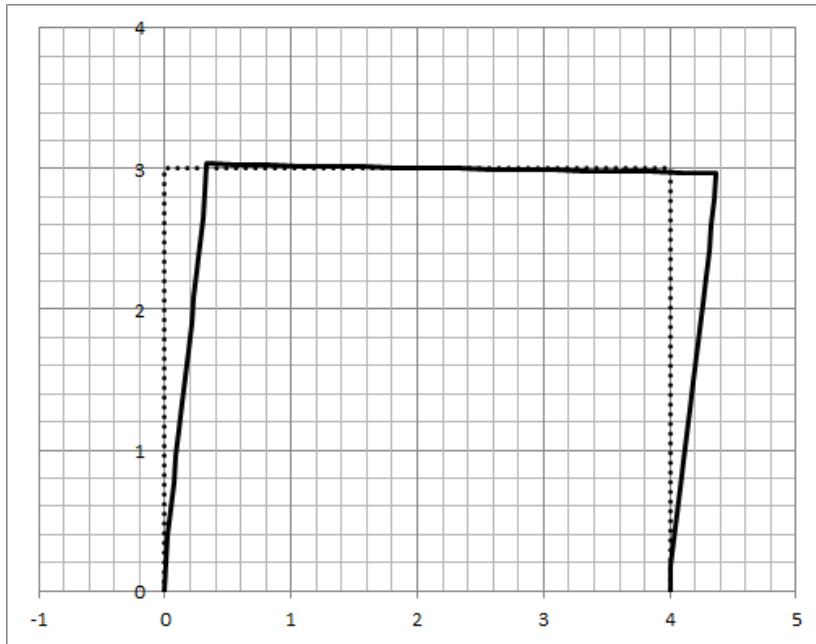
Figure 4.37 Deformed shape after lateral loading (magnified 5 times)
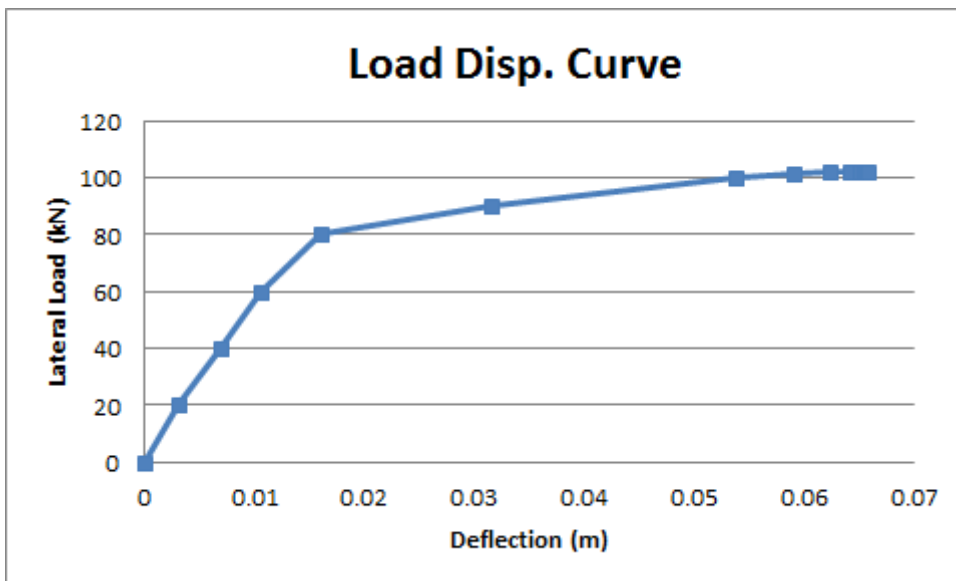
Figure 4.38 Load displacement curve for FA test case.

In Figure 4.38, the displacement of the node is given for each load increment. The frame displays linear behavior until 80 kN transverse load. After 80 kN loading, the plastic hinges are formed and the nonlinear behavior is displayed.

As the later load is being applied, the axial loading in the columns change. At each load increment the axial forces are updated for every member in the frame. A new section response is calculated according to the updated axial loading.

In Figure 4.39, the change of curvatures is plotted. The initial load increments do not cause any nonlinear behavior. Up to 87.6 kN lateral loading, the curvatures along the columns are small, in other words, the behavior of the frame is still linear. At 87.6 kN lateral load, at the support regions of the columns, the curvatures increases dramatically. It shows that the first and the second plastic hinges form simultaneously at support region. After the formation of

the first plastic hinge couples, the frame keeps carrying the load. At 98.6 kN lateral load, the curvatures at beam-column connection area increases. The third and fourth plastic hinges are formed at beam-column connection points. Due to the plastic hinges, the frame stiffness softens, thus the large displacements occur. Also, it is clear that the behavior of the left column is similar to the right column.
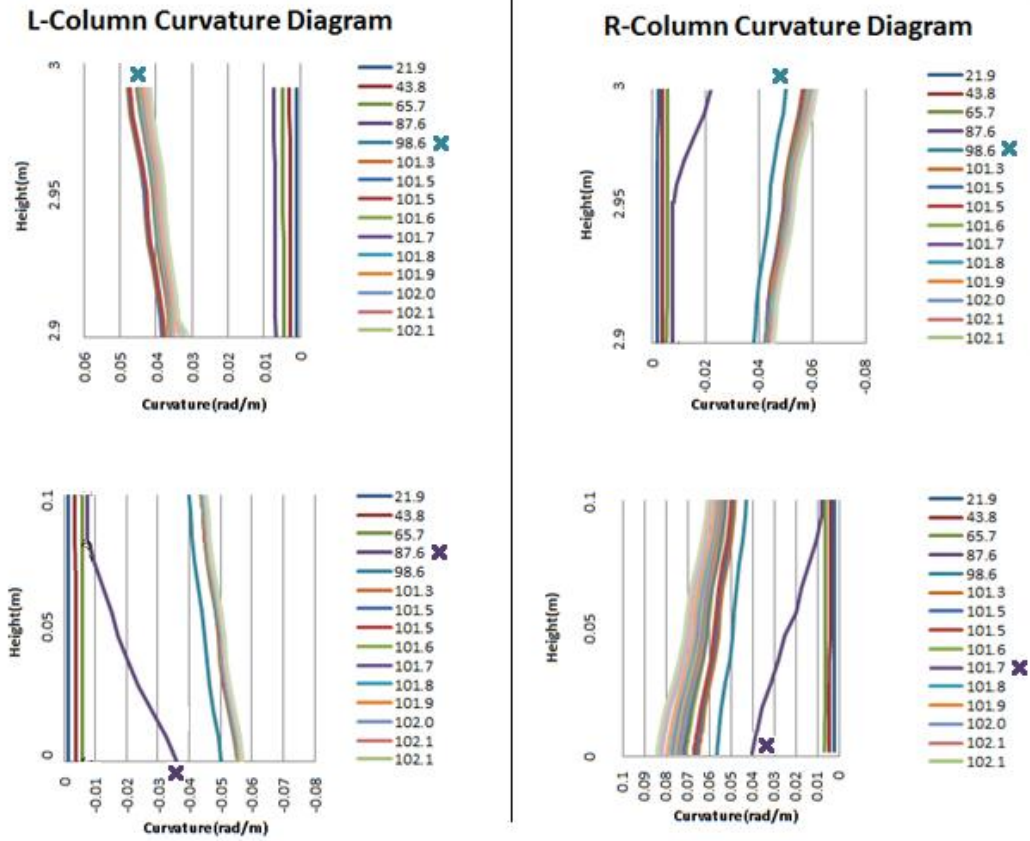
Figure 4.39 Curvature diagrams at support and connection points for the FA test case.

CHAPTER 5

SUMMARY, CONCLUSION AND RECOMMENDATIONS

5.1 Summary

Reinforced concrete is one of the most important building materials for the construction industry. It is composed of concrete and steel, and displays nonlinear behavior. The main reason of nonlinearity is the concrete itself and its composite nature. The concrete consists of non-homogenous compounds and has anisotropic behavior. Additional nonlinearity is introduced by reinforcing bars. Some of the bars are used as straight bars, but according to the moment diagram, some bars might be selected as bent bars. In other words, the steel configuration changes throughout the beam length, causing nonlinearity by changing element's flexural rigidity EI. For the sake of simplicity, usually the linear analysis is conducted for design purposes. Nonlinear analysis consumes more time for the calculation and harder to model. Various studies and solution techniques are suggested by researchers by different material models and finite element types. Mainly, brick elements or quadrilateral elements are available in the literature. Two node Hermitian beam element is selected for this study, because it has fewer nodes than other finite element types and has a superior flexural behavior.

In this study, the RC beams are modeled by using two node beam element. For the section analysis, it is assumed that the section does not change under loadings, in other words, a perfect bond is formed between concrete and reinforcing bars. The second assumption is that the plane sections remain plane. This assumption comes from the Euler-Bernoulli beam theory. According to this assumption, the shear deformations are neglected. The Hermitian functions are selected as shape functions. Due to the order of the shape functions, the change of curvature cannot be calculated exactly, that is why as the mesh size increases, the solution converges to the exact solution. The element stiffness is calculated by taking average of the stiffness contributions at each integration point along the element. For a given displacement, the curvatures are calculated at integration points and the stiffness matrix of the element is constructed. Then, a new deformed configuration is calculated by using this stiffness. This iterative procedure is continued until convergence is attained.

A program is developed for the analysis of reinforced concrete frames and it is coded in C++. For the analysis, several properties should be defined in the program. Firstly, the material properties should be defined. Then, the sections should be defined in terms of the dimensions of the section, the number of steel bars and their sizes and depths. Then, the connectivity of the elements should be defined. Start and end joints of elements and the type of section used throughout the element should also be defined. Lastly, the applied load is given and the analysis is started.

The verification of the analysis results is done by comparing them with the test results. It is seen that the behavior of the beams under loading is similar to those in the experiments. The observed difference between the analytical and the test results is believed to be caused by the assumptions stated above. The resulting internal forces and the section capacities are consistent with each other.

5.2 Conclusion

The following conclusions are drawn based on experience gained and the analysis results obtained in this study.

- The analytical procedure proposed in this study is effective in predicting the nonlinear behavior of RC frame structures under loads. This is verified by the close agreement between the analytical predictions and the test results.

- The analytical tool developed in this study makes it possible to observe the formation and location of plastic hinges as well as the shifting of the inflection points along the frame elements as the loading increases. When the internal moment reaches the section capacity at any point along the member, the curvature at the point increases very rapidly indicating the formation of a plastic hinge.
- Higher mesh densities should be used for accurate internal forces. In this case, less integration points can be used. As the length of the element decreases, the change in the stiffness at each integration point also decreases. This, in turn, decreases the computation time.

5.3 Recommendations for Future Studies

Based on the experience gained in this study, it is seen that there are certain aspects of the approach suggested which needs to be improved for a more efficient and accurate analysis. Some of these improvements are in the theoretical and modeling approach and some of them are in the program itself.

- The reinforcing bars are assumed to be perfectly bonded to concrete. The bond-slip behavior between these two materials can be taken into account for more accurate results.
- The Newton Raphson solution algorithm can be complemented by an arc-length method to obtain the post yielding behavior of structures.
- The section is modeled by using longitudinal bars only. The effect of stirrups must be included for a better accuracy.
- Currently, the shear deformations are assumed to be negligible. This effect must be included.
- The code can be optimized in terms of time and efficiency.
- The program has no user interface. A graphical user interface would facilitate the description and the modeling of the RC structure.
- The program has no save, load and restart mechanism. Considering the length of solution time, this is very useful especially in the case of uncontrolled interruption of the execution.

REFERENCES

[1]   Hognestad, E. (1951). "A Study of Combined Bending and Axial Load in Reinforced Concrete Members". University of Illinois Engineering Experiment Station, Bulletin Series No. 399, Bulletin No. 1.

[2]   Ngo, D. and Scordelis, A.C. (1967). "Finite Element Analysis of Reinforced Concrete Beams," Journal of ACI, Vol. 64, No. 3, pp. 152-163.

[3]   Tasuji, M.E., Slate, F.O. and Nilson, A.H. (1978). "Stress-Strain Response and Fracture of Concrete in Biaxial Loading". Journal of ACI, Vol. 75, No. 3, pp. 306-312.

[4]   Gupta, A.K. and Akbar, H. (1983). "A Finite Element for the Analysis of Reinforced Concrete Structures". International Journal for Numerical Methods in Engineering, Vol. 19, pp. 1705-1712.

[5]   Kwak, H. G. and Filippou, F.C.(1990)."Finite Element Analysis of Reinforced Concrete Structures Under Monotonic Loads". Department of Civil Engineering University of California

[6]   H. G. Kwak and Sun-Pil Kim(2000)."Nonlinear Analysis of RC Beams Based on Moment Curvature Relation". Department of Civil and Environmental Engineering, Korea Advanced Institute of Science and Technology

[7]   K. Phuvoravan (2003),"A Finite Element for the Nonlinear Analysis of Reinforced Concrete Slabs", PhD thesis, Prude University, West Lafayette, Indiana

[8]   U. Ersoy, G. Ozcebe and T. Tankut(2003), "Reinforced Concrete", Ankara, (pp. 197-198)

[9]   K.J. Thompson and R. Park(1978), "Stress-Strain Model for Grade 275 Reinforcing Steel with Cyclic Loading", Bulletin of the New Zealand National Society for Earthquake Engineering Vol. 11,No 2, pp. 101-102

APPENDIX A

PARAMETRIC STUDIES

The structural analysis of a beam element can be performed in several ways. The mesh size is an important parameter for nonlinear analysis. To achive accurate results, the mesh size should be high enough to approximate the behaviour of the element. On the other hand, the usage of more mesh size means an increase in computational time. Thus, a proper mesh size should be selected. As well as the mesh size, the number of integration points effects the analysis results. Troughout the analysis, integrations are calculated numericaly, thus, the accuracy of the integrations depends on the integration points. Usage of more integration points also increases the computation time.
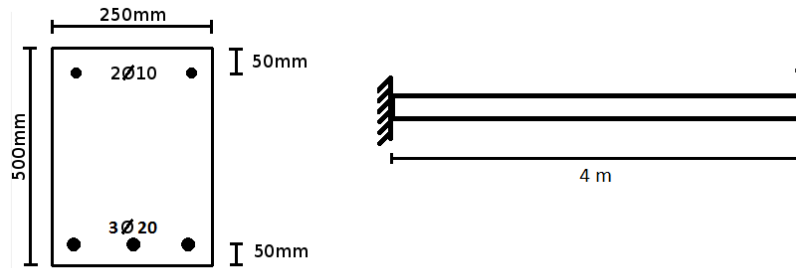
Figure A.1 Dimensions and section geometry for CPL2 test case

Concrete and steel material parameters:

f_c = 50 MPa

ε_{co} = 0.002

ε_{cu} = 0.003

ε_{sy} = 0.0021

ε_{sh} = 0.0105

f_y = 420 MPa

f_u = 630 MPa

E_s = 200 GPa

The concrete model is selected as Hognestad concrete model and the steel model is selected as Kent & Park's steel model.

To compare the effects of mesh size and integration point selection, a cantilever RC beam with a point load is analyzed. Three parameters are compared; tip deflection, support moments and the computation time. In Table A.1, A.2 and A.3 these parameters are listed respectively.

Table A.1 Table of tip displacements

Tip Displacement(m)		n		
		16	32	64
Integration points	2	0.127	0.121	0.119
	5	0.121	0.119	0.118
	10	0.122	0.119	0.117

Table A.2 Table of support moments

Support Reaction(kNm)		n		
		16	32	64
Integration points	2	-198.47	-196.77	-196.13
	5	-197.93	-197.15	-196.42
	10	-197.99	-196.61	-196.79

Table A.3 Table of computation times

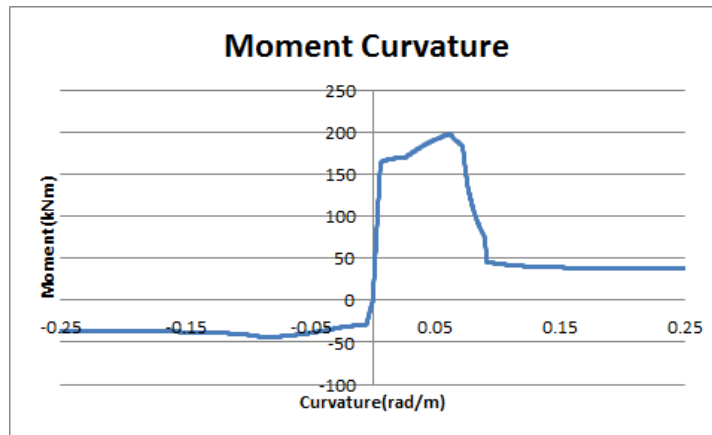| Time(t)		n		
		16	32	64
Integration points	2	1.0	2.1	4.7
	5	1.8	3.7	8.5
	10	3.4	6.7	14.7

Figure A.2 Moment curvature diagram of the CPL2 test case's section

In Figure A.2, moment curvature diagram of the section is given. The moment capacity of the section is 197.8 kNm. In Table A.1, the tip displacements of the cantilever beam is listed. For 16 element mesh, the diplacement changes dramatically as the integration point increases. For 32 and 64 element meshes, the displacement does not change as the integration point increases. On the other hand, the support moments give more information about the nonlinear behaviour of the member. All integration point combinations for the 16 element mesh size exceed the allowable moment capacity. For 32 element mesh size, all results are smaller than the moment capacity, but still the forces vary as the integration point changes. The 64 element mesh displays more stable changes; as the integration point increases, the forces converge.

In Table A.3, the computation times of the analyses are listed. Increase of both integration points and mesh sizes increases computation time. 32 and 64 mesh size gives similar results in terms of forces and displacements. On the other hand, using higher mesh size always gives better approximation. The results of 32 mesh size with 10 integration points and 64 mesh size with 2 integration points give very close results in terms of displacements and forces. Due to the increase of integration points, the computation time of 32 element mesh size is higher than the 64 element mesh size anaysis.To sum up, increasing the mesh size is more effective than increasing the integration points.

APPENDIX B

GAUSS-LEGENDRE INTEGRATION CONSTANTS

Table B.1 Gauss–Legendre quadrature table

Number of Points, n	Points, x_i	Weights, w_i	Number of Points, n	Points, x_i	Weights, w_i
1	0.000	2.000		-0.960	0.101
				-0.797	0.222
2	-0.577	1.000		-0.526	0.314
	0.577	1.000		-0.183	0.363
			8	0.183	0.363
3	-0.775	0.556		0.526	0.314
	0.000	0.889		0.797	0.222
	0.775	0.556		0.960	0.101
4	-0.861	0.348		-0.968	0.081
	-0.340	0.652		-0.836	0.181
	0.340	0.652		-0.613	0.261
	0.861	0.348		-0.324	0.312
			9	0.000	0.330
5	-0.906	0.237		0.324	0.312
	-0.538	0.479		0.613	0.261
	0.000	0.569		0.836	0.181
	0.538	0.479		0.968	0.081
	0.906	0.237			
				-0.974	0.067
6	-0.932	0.171		-0.865	0.149
	-0.661	0.361		-0.679	0.219
	-0.239	0.468		-0.433	0.269
	0.239	0.468		-0.149	0.296
	0.661	0.361	10	0.149	0.296
	0.932	0.171		0.433	0.269
				0.679	0.219
7	-0.949	0.129		0.865	0.149
	-0.742	0.280		0.974	0.067
	-0.406	0.382			
	0.000	0.418			
	0.406	0.382			
	0.742	0.280			
	0.949	0.129			